NOTICE

The quality of this microform is heavily dependent upon the quality of the original thesis submitted for microfilming. Every effort has been made to ensure the highest quality of reproduction possible.

If pages are missing, contact the university which granted the degree.

Some pages may have indistinct print especially if the original pages were typed with a poor typewriter ribbon or if the university sent us an inferior photocopy.

Previously copyrighted materials (journal articles, published tests, etc.) are not filmed.

Reproduction in full or in part of this microform is governed by the Canadian Copyright Act, R.S.C. 1970, c. C-30.

AVIS

La qualité de cette microforme dépend grandement de la qualité de la thèse soumise au microfilmage. Nous avons tout fait pour assurer une qualité supérieure de reproduction.

S'il manque des pages, veuillez communiquer avec l'université qui a conféré le grade.

La qualité d'impression de certaines pages peut laisser à désirer, surtout si les pages originales ont été dactylographiées à l'aide d'un ruban usé ou si l'université nous a fait parvenir une photocopie de qualité inférieure.

Les documents qui font déjà l'objet d'un droit d'auteur (articles de revue, tests publiés, etc.) ne sont pas microfilmés.

La reproduction, même partielle, de cette microforme est soumise à la Loi canadienne sur le droit d'auteur, SRC 1970, c. C-30.

Canada

On the Stream Function Solution of Inviscid Transonic Flow Problems

Viswanath Rao Tata

A Thesis

in

The Department

of

Mechanical Engineering

Presented in Partial Fulfillment of the Requirements
for the Degree of Master of Engineering at
Concordia University
Montréal, Québec, Canada

June 1988

ISBN 0-315-44864-4

ABSTRACT

On the Stream Function Solution of Inviscid Transonic Flow Problems

Viswanath Rao Tata

The numerical calculation of the transonic flowfields encountered in aircraft and turbomachinery applications is essential in predicting the aerodynamic behaviour of these components. In this Thesis a stream function based method is presented for the solution of inviscid transonic flows for such geometries. It has the advantage over the velocity potential method in being able to calculate rotational flows with strong shock waves.

Some aspects of the stream function formulation are addressed in order to make it a more efficient and practical method. The difficulty of obtaining the density due to the double-valuedness of the mass flux versus Mach number for transonic flows is overcome with three different approaches. In the first method the density is obtained by solving the first order vorticity definition equation. In the second approach the first order vorticity equation is recast as a second order equation. In the third, a second order equation for pressure is solved and the density is obtained from the energy equation thereby avoiding the double-valuedness problem.

Efficient solution methods are addressed and the Zebroid method, an alternating horizontal line relaxation algorithm, is developed in the finite element context and reduces the computational effort for the solution.

The results obtained for transonic flow over isolated airfoils and unchoked compressor cascades show that the stream function method is an effective approach.

ACKNOWLEDGEMENTS

The author wishes to thank his thesis supervisor, Dr. W.G. Habashi for his guidance and encouragement during this research.

In addition, the valuable technical assistance and support provided by the author's colleagues Messrs. B. Nguyen, G. Guevremont and A. Cion is greatly appreciated. Special thanks go out to Ms. P. Lavery for typing this manuscript.

The financial support of the Natural Sciences and Engineering Research Council of Canada through an NSERC Graduate Scholarship is gratefully acknowledged.

TABLE OF CONTENTS

NOMENCLATURE

a	speed of sound
E	internal energy
f	right-hand side vector
h	enthalpy
K	global influence matrix
k	element influence matrix
M	Mach number
N	shape function
p	pressure
q	velocity, $\sqrt{u^2 + v^2}$
R	residual
s	distance along a streamline
T	temperature
u,v	Cartesian velocity components
x,y	Cartesian coordinates
W	weight function
α,β	relaxation factors
γ	isentropic exponent
δ,Δ	change in a quantity
Φ	velocity potential
Ψ	stream function
μ	artificial compressibility coefficient
ρ	density
$\tilde{\rho}$	artificial compressibility
ω	vorticity

Subscripts

e,e-1	element, upstream element
i,j	nodal indices
n	outward normal direction
o	stagnation property
x,y,t	derivatives with respect to x, y, time
∞	free-stream value

LIST OF FIGURES

CHAPTER 1

INTRODUCTION

1.1 The Transonic Flow Problem

The use of computational methods to simulate the behaviour of fluid flows has increased rapidly during the past decade. This is due to the rapid progress in computer technology and the ever-increasing requirements to improve the aerodynamic efficiency of aircraft and turbomachines. While the motion of a fluid that is unsteady, three-dimensional, viscous and compressible is governed by the Navier-Stokes equations; many flow situations of practical interest can be well approximated by the interaction of inviscid and boundary layer solutions.

This Thesis addresses in particular two-dimensional transonic inviscid flow problems. The Mach number range just above the drag-rise Mach number, M_d, is known to be one of the most efficient regimes of flight, and it is this feature that makes the analysis of transonic flow fields one of the most studied problems in fluid dynamics. As the free-stream Mach number increases beyond the optimum performance range, adverse effects in the form of increased drag, shock-induced separation, and buffet are encountered. The onset of these phenomena can impose limitations on the operating Mach number range of airplanes, helicopter rotors, propellers, inlets and compressors. It is thus clear that understanding and predicting this behaviour is important.

Some of the early pioneering work done in the area of computational transonics involved the solution of the transonic small disturbance (TSD) equation for the velocity potential, given by:

$$[\,1 - M_\infty^2 - (\gamma + 1)\,\Phi_x\,]\,\Phi_{xx} + \Phi_{yy} = 0 \qquad (1.0\,a)$$

This equation applies to airfoils with small thickness-to-chord ratios. Murman and Cole's breakthrough in 1970 [1] involved a mixed finite-difference scheme applied to the

TSD equation. In their method, central differences were applied in subsonic flow regions and backward differences in supersonic flow regions in order to satisfy the domain of dependence restriction for the partial differential equation. Furthermore, their line implicit formulation helped to avoid numerical instability problems in supersonic zones.

The introduction of the shock-point operator by Murman [2] yielded a fully flux-conservative scheme for the TSD equation, with shocks that were stronger and farther downstream than those of non-conservative approaches. Non-conservative results, however, seemed to bear a closer resemblance to the physical flow than conservative ones, as shown by Newman and South in [3].

This original research led the way to rapid progress in the field. In the early to mid-sixties, experimental aerodynamicists such as Pearcy [4] of NPL and Whitcomb [5] of NASA began developing airfoil sections which produced essentially shock-free flows, leading analysts such as Garabedian, Korn and Bauer [6] to deal with supercritical airfoils having round noses and peaky pressure distributions by tackling the full potential equation (FPE) in non-conservative form:

$$(a^2 - \Phi_x^2)\,\Phi_{xx} - 2\Phi_x\Phi_y\Phi_{xy} + (a^2 - \Phi_y^2)\,\Phi_{yy} = 0 \qquad (1.0\,b)$$

They also successfully adapted a turbulent boundary layer model into their FPE code. The need to apply the FPE to practical, swept, three-dimensional wings led to the significant contribution by Jameson in his rotated-difference scheme [7]. In that scheme, the FPE is rewritten in conservative form in a local Cartesian coordinate system (s,n) oriented along the streamline and normal to it:

$$(1 - M^2)\,\Phi_{ss} + \Phi_{nn} = 0 \qquad (1.0\,c)$$

where

$$\Phi_{ss} = \frac{u^2}{q^2}\Phi_{xx} + \frac{2uv}{q^2}\Phi_{xy} + \frac{v^2}{q^2}\Phi_{yy}$$

$$\Phi_{nn} = \frac{v^2}{q^2}\Phi_{xx} - \frac{2uv}{q^2}\Phi_{xy} + \frac{u^2}{q^2}\Phi_{yy}$$

Centered differences are utilized for all terms except when upwinding is used for Φ_{ss} at points where $M > 1$.

Steger and Lomax were among the first to produce solutions to the FPE for two-dimensional lifting airfoils [8], while some of the earliest results for three-dimensional flows came from Steger and Bailey [9]. Efforts directed at improving the solution efficiency included algorithms such as the multigrid (MG) method introduced by South and Brandt [10] and the approximate factorization method by Ballhaus et al. [11]. Eberle [12] and Hafez [13] were the first to incorporate the dissipation needed in the scheme via an upwind shift of the density, the first in a finite-element approach and the latter in finite differences. At about the same time, finite-difference formulations of this method were also introduced by Holst and Ballhaus [14], and Purvis and Burkhalter [15].

The stream function approach to the transonic flow problem was successfully initiated by Emmons [16], who solved for rotational flows using the stream function/vorticity approach and shock fitting. Shock capturing attempts to solve the stream function equation failed, however, because the density is not uniquely determined in terms of mass flux; there are two solutions, one is subsonic and the other supersonic with a square root singularity at the sonic point. The stream function solution is preferred in applications where the exact conservation of mass is important such as in internal and turbomachinery flows. Furthermore, the capability of the method to calculate the vorticity generated by shock waves is another advantage of the stream function over the velocity potential. The pioneering paper of Hafez and Lovell [17] presented a method of overcoming the singularity problem for finite difference solutions

of external flow problems. The impetus behind the current work is to extend the applicability of the method to internal flows , in a finite element context.

1.2 Governing Equations for Two-Dimensional Inviscid Transonic Flows

The governing equations for two-dimensional, compressible, inviscid flow are the continuity and the vorticity definition equations, where:

(1) Continuity Equation:

$$\frac{\partial}{\partial x}(\rho u) + \frac{\partial}{\partial y}(\rho v) = 0 \qquad (1.1)$$

(2) Vorticity Definition Equation:

$$\frac{\partial u}{\partial y} - \frac{\partial v}{\partial x} = \omega \qquad (1.2)$$

with the vorticity ω given by the Crocco relation

$$q \cdot \underline{\omega} = T \cdot \frac{\partial s}{\partial n} \qquad (1.3)$$

This expression yields the vorticity in terms of the gradient of entropy across streamlines. Equations (1.1) and (1.2) have been derived from the equations for conservation of mass, momentum and energy for steady, isentropic flow of a perfect gas. In this Thesis, the vorticity generated by the presence of strong shock waves has been neglected. Therefore, equation (1.2) may be rewritten as:

$$\frac{\partial u}{\partial y} - \frac{\partial v}{\partial x} = 0 \qquad (1.4)$$

The energy equation provides the relationship between the density and Mach number as follows:

$$\frac{\rho}{\rho_o} = \left[1 - \frac{\gamma - 1}{2} M_o^2 \right]^{1/(\gamma-1)} \qquad (1.5)$$

where $M_o = q/a_o$, the Mach number with respect to the stagnation speed of sound.

In summary, the system of governing equations to be solved are (1.1), (1.4) and (1.5).

1.3 The Stream Function Approach

The stream function, Ψ, is defined to satisfy the continuity equation identically:

$$u = \frac{1}{\rho}\frac{\partial \Psi}{\partial y} \tag{1.6a}$$

$$v = -\frac{1}{\rho}\frac{\partial \Psi}{\partial x} \tag{1.6b}$$

The governing equation is thus obtained upon substitution into the vorticity equation (1.4):

$$\frac{\partial}{\partial x}\left(\frac{1}{\rho}\frac{\partial \Psi}{\partial x}\right) + \frac{\partial}{\partial y}\left(\frac{1}{\rho}\frac{\partial \Psi}{\partial y}\right) = 0 \tag{1.7}$$

The energy equation, rewritten in terms of Ψ is hence:

$$\frac{\rho}{\rho_o} = \left[1 - \frac{\gamma - 1}{2}\left(\frac{\nabla \Psi}{a_o \rho}\right)^2\right]^{1/(\gamma-1)} \tag{1.8}$$

The stream function scheme, then, lies in the solution of equations (1.7) and (1.8). The main advantages of this formulation over the Euler equations in primitive variables form [18] are:

(1) only one variable, rather than four, need to be solved for;

(2) the second-order stream function equation has simpler boundary conditions than the set of first-order Euler ones.

(3) the stream function guarantees the exact conservation of mass.

The strong points of this method when compared to the velocity potential approach [19] are in its ability to include the rotational effects due to entropy gradients behind curved shocks, and to its Dirichlet boundary conditions over solid bodies.

However, this model is not without its difficulties. For transonic flows, the density-mass flux relation becomes double-valued, as shown in Figure 1.1. For a given value of mass flux (ρq), two values of density are possible, one corresponding to a subsonic Mach number and the other to a supersonic one. For the nonlinear problem at hand, this leads to convergence difficulties in the iterative scheme at high Mach numbers.

This non-uniqueness issue has been resolved in [20] for the finite difference solution of external flow problems. The first-order vorticity equation is used to calculate the velocity q once the stream function distribution (hence the flow orientation) is known. The flow angle, θ, at any point in the field can be expressed as:

$$\theta = \tan^{-1}\left(\frac{v}{u}\right) = \tan^{-1}\left(\frac{\rho v}{\rho u}\right) = \tan^{-1}\left(\frac{-\Psi_x}{\Psi_y}\right) \qquad (1.9)$$

The vorticity definition equation can hence be rewritten as:

$$\frac{\partial u}{\partial y} - \frac{\partial v}{\partial x} \equiv \frac{\partial}{\partial y}(q\cos\theta) - \frac{\partial}{\partial x}(q\sin\theta) = 0 \qquad (1.10)$$

where $q = \sqrt{u^2 + v^2}$ and the only unknown is q.

Equation (1.10) is integrated to evaluate q marching in the general direction of the characteristic. The solution must start from an initial data line other than a characteristic, and, for isolated airfoils, this data line can be taken to be the far-field boundary representing the free stream. Once q is determined, the density is updated using the energy equation (1.8). For internal and cascade flows the problem of the initial data line is obviously more complex and Chapter 3 presents a new algorithm suitable to internal flow problems.

A brief mention of the classification of partial differential equations at this

point is essential. The general characteristic form of a second order partial differential equation is:

$$A(.)\, u_{xx} + 2B(.)\, u_{xy} + C(.)\, u_{yy} = D(.) \qquad (1.11)$$

Here, A, B, C, D are functions of x, y, u_x, u_y and the coefficient (B^2 - AC) determines the nature of the equation, i.e., the existence or not of characteristics. Characteristic lines possess the following properties, among others:

(1) These are the directions of propagation of signals, i.e., while across these the function u is continuous its slope is discontinuous.

(2) If initial data is given on a characteristic, it is hence impossible to continue the solution by stepping off this line.

The direction of the two characteristics corresponding to the general second-order PDE is:

$$\left(\frac{dy}{dx}\right)_{1,2} = \frac{-B \pm \sqrt{B^2 - AC}}{A} \qquad (1.12)$$

and if $B^2 - AC < 0$ PDE is elliptic

$B^2 - AC = 0$ PDE is parabolic

$B^2 - AC > 0$ PDE is hyperbolic.

For elliptic equations the characteristics are imaginary, i.e., they do not exist. Physically, this means that disturbances propagate equally in all directions and an observer standing somewhere in the flow can feel disturbances emanating upstream and downstream of his position. In the case of hyperbolic equations, two real characteristics exist, across which a discontinuous slope is permitted. Two important regions can be defined:

(1) <u>domain of dependence</u> - any disturbances felt by the observer originate from downstream points contained within the region defined by the two characteristics arriving at his position.

(2) <u>domain of influence</u> - any disturbances created by the observer can only

be felt at upstream points contained within the region defined by the two characteristics emanating from his position.

Finally, for parabolic equations, the two characteristics collapse onto one. Thus, an observer standing in a flow described by a parabolic equation is affected by all disturbances created previously and his zone of influence extends to all points in the upstream domain.

Transonic flows are elliptic in subsonic regions, parabolic across the sonic line, and hyperbolic at supersonic points. The governing equations are hence said to be of "mixed" type. In order to illustrate this, let us recast the stream function equation in non-conservative form:

$$\left[1 - \left(\frac{\rho_o}{\rho}\right)^2 \frac{\Psi_y^2}{a^2}\right] \Psi_{xx} + \left[1 - \left(\frac{\rho_o}{\rho}\right)^2 \frac{\Psi_x^2}{a^2}\right] \Psi_{yy} + 2\left(\frac{\rho_o}{\rho}\right)^2 \frac{\Psi_x \Psi_y}{a^2} \Psi_{xy} = 0$$

For this equation,

$B^2 - AC < 0$ if $q < a$; SUBSONIC FLOW, equation is ELLIPTIC

$= 0$ if $q = a$; SONIC LINE, equation is PARABOLIC

> 0 if $q > a$; SUPERSONIC FLOW, equation is HYPERBOLIC

1.4 Finite Element Discretization

In this section, the finite element formulation of the two-dimensional stream function equation will be presented.

1.4.1 The Galerkin "Weak" Formulation

Let us consider a general partial differential equation (PDE) of the form:

$$L(u) = f \qquad (1.13)$$

In the method of weighted residuals, the desired function u is replaced by a

finite series approximation $\hat{u}$,

$$u \approx \hat{u} = \sum_{j=1}^{N} u_j N_j \qquad (1.14)$$

In general, the set of functions N_j, j = 1,2,...,N, known as the basis or interpolation functions are defined over the element domain and u_j, j = 1,2,...,N, are the undetermined coefficients. Even when the basis functions are chosen to satisfy all boundary conditions imposed on a problem, they will not normally satisfy the PDE as well. Substitution of $\hat{u}$ into the PDE, L(u) - f = 0, results in a residual, R,

$$L(\hat{u}) - f = R \qquad (1.15)$$

The objective is to select the undetermined coefficients u_j such that this residual is minimized in some sense. This can be accomplished by setting the weighted residual to zero as:

$$\iint_A [\, L(\hat{u}) - f \,] W_i \, dx \, dy = 0 \qquad (1.16)$$

In the Galerkin Weighted Residual Method, the weighting functions W_i are chosen to be the basis functions N_i themselves. Thus one obtains:

$$\iint_A [\, L(\hat{u}) - f \,] N_i \, dx \, dy = 0 \qquad (1.17)$$

The finite element approximation to (1.17) is in breaking the integral into its sum over all the elements:

$$\sum_{i=1}^{E} \iint_{A_i} [\, L(\hat{u}) - f \,] N_i \, dx \, dy = 0 \qquad (1.18)$$

where E is the number of elements.

1.4.2 Isoparametric Elements

In the isoparametric finite element approach, elements of irregular shape are

transformed or mapped into elements of regular geometry to facilitate integration. Consider an irregularly shaped four-noded quadrilateral element as shown in Figure 1.2. This can be transformed into the regular-shaped element illustrated in the same figure using mapping functions. Within an element, the function f and the coordinates (x,y) are given by:

$$f = \sum_{i=1}^{DOF} M_i(\xi, \eta)\, f_i \tag{1.19a}$$

$$x = \sum_{i=1}^{DOF} N_i(\xi, \eta)\, x_i \tag{1.19b}$$

$$y = \sum_{i=1}^{DOF} N_i(\xi, \eta)\, y_i \tag{1.19c}$$

Here (ξ, η) are the non-dimensional coordinates of the undistorted element, (x_i, y_i) are the global coordinates of node i, and DOF represents the number of degrees of freedom. Isoparametric elements are ones in which the order of the geometric interpolation function N_i and the field interpolation function M_i are the same.

In the case of four-node isoparametric bilinear elements, the geometric interpolation function N_i can be expressed as:

$$N_i(\xi, \eta) = \frac{1}{4}(1 + \xi\,\xi_i)(1 + \eta\,\eta_i) \tag{1.20}$$

It is readily apparent that N_i is unity at node i and varies linearly along ξ ($\eta = \pm 1$), and along η ($\xi \pm 1$). The variation within the element, however, is bilinear.

1.4.3 Stream Function Equation in Discretized Form

Applying the Galerkin Weighted Residual Method to the stream function equation (1.7), we obtain:

$$\sum_{i=1}^{E} \iint_{A_e} \left[\frac{\partial}{\partial x}\left(\frac{1}{\rho}\frac{\partial \Psi}{\partial x}\right) + \frac{\partial}{\partial y}\left(\frac{1}{\rho}\frac{\partial \Psi}{\partial y}\right) \right] dx\, dy = 0 \qquad (1.21)$$

This can be integrated by parts using Green's theorem:

$$\iint u \cdot \nabla v \, dA = \int u\,(v.n)\, ds - \iint v.\nabla u \, dA \qquad (1.22)$$

to get:

$$-\iint_{A_e} \left[\frac{1}{\rho}\frac{\partial \Psi}{\partial x}\frac{\partial N_i}{\partial x} + \frac{1}{\rho}\frac{\partial \Psi}{\partial y}\frac{\partial N_i}{\partial y} \right] dxdy + \int N_i \frac{1}{\rho}\frac{\partial \Psi}{\partial n} ds = 0 \qquad (1.23)$$

Using the fact that

$$\frac{\partial \Psi}{\partial x} = \sum_{i=1}^{DOF} \frac{\partial N_i}{\partial x} \Psi_i \qquad (1.24a)$$

$$\frac{\partial \Psi}{\partial y} = \sum_{i=1}^{DOF} \frac{\partial N_i}{\partial y} \Psi_i \qquad (1.24b)$$

and assuming that the density is constant over each element, equation (1.23) becomes

$$-\frac{1}{\rho_e} \iint \left[\frac{\partial N_i}{\partial x}\frac{\partial N_j}{\partial x} + \frac{\partial N_i}{\partial y}\frac{\partial N_j}{\partial y} \right] dxdy \{\Psi\} + \int N_i \frac{1}{\rho}\frac{\partial \Psi}{\partial n} ds = 0 \qquad (1.25)$$

Assembly of the area integrals at the element level yields the element influence matrix [k], which is a square matrix of order four with elements

$$k_{\Psi ij} = \frac{1}{\rho_e} \iint_{A_e} \left[\frac{\partial N_i}{\partial x}\frac{\partial N_j}{\partial x} + \frac{\partial N_i}{\partial y}\frac{\partial N_j}{\partial y} \right] dx\, dy$$

The derivatives are evaluated numerically at the local, or element level and subsequently mapped to the global coordinate system:

$$\begin{bmatrix} \frac{\partial N_i}{\partial \xi} \\ \frac{\partial N_i}{\partial \eta} \end{bmatrix} = \begin{bmatrix} \frac{\partial x}{\partial \xi} & \frac{\partial y}{\partial \xi} \\ \frac{\partial x}{\partial \eta} & \frac{\partial y}{\partial \eta} \end{bmatrix} \begin{bmatrix} \frac{\partial N_i}{\partial x} \\ \frac{\partial N_i}{\partial y} \end{bmatrix} = [J] \begin{bmatrix} \frac{\partial N_i}{\partial x} \\ \frac{\partial N_i}{\partial y} \end{bmatrix} \qquad (1.27)$$

where

$$\frac{\partial x}{\partial \xi} = \sum_{i=1}^{DOF} \frac{\partial N_i}{\partial \xi} x_i$$

$[J]$ = Jacobian matrix

The global derivatives are given by:

$$\begin{bmatrix} \frac{\partial N_i}{\partial x} \\ \frac{\partial N_i}{\partial y} \end{bmatrix} = [J]^{-1} \begin{bmatrix} \frac{\partial N_i}{\partial \xi} \\ \frac{\partial N_i}{\partial \eta} \end{bmatrix} \qquad (1.28)$$

The element integrals may be evaluated by using (2×2) Gaussian quadrature [21];

$$K = \int_{-1}^{1}\int_{-1}^{1} F(\xi,\eta) |J| \, d\xi \, d\eta$$

$$= \sum_{i=1}^{NG} \sum_{j=1}^{NG} W_i W_j F(\xi_i,\eta_j) |J(\xi_i,\eta_j)| \qquad (1.29)$$

where NG is the order of integration (2 in this case)

W_i, W_j are weighting factors ($W_i = W_j = 1$ for (2×2) integration)

(ξ_i, η_j) are the local coordinates of the Gaussian integration points

The traditional finite element assembly technique is applied to form the overall global influence matrix, yielding the governing matrix system:

$$[K_\Psi] \{\Psi\} = \{F_\Psi\} \qquad (1.30)$$

with

$$[K_\Psi] = \sum_{e=1}^{E} k_{\Psi ij}$$

$$F_{\Psi,i} = \int \frac{1}{\rho} N_i \frac{\partial \Psi}{\partial n} ds$$

The iterative problem is subsequently handled using the methods described in Section 1.6.

1.5 Some Aspects of the Numerical Treatment of Transonic Flows

Certain aspects of the transonic flow problem necessitate the use of special numerical treatment, and these are introduced here.

1.5.1 Artificial Compressibility Method

The physics of supersonic flow dictate that the effect of a moving particle is felt only within a zone bounded by Mach lines upstream of the particle. This is in contrast to subsonic flow, in which the disturbance caused by a particle is sensed in all directions. Therefore, numerical schemes for transonic flows must account for the fact that the domain of influence in supersonic regions is limited to upstream points. So-called backward or upwind differencing must be applied at all supersonic points. Another way of looking at this is by first considering the full-potential equation written in non-conservative form:

$$(a^2 - u^2)\,\Phi_{xx} - 2\,uv\Phi_{xy} + (a^2 - v^2)\,\Phi_{yy} = 0 \qquad (1.31)$$

where

$$u = \frac{\partial \Phi}{\partial x}, \qquad v = \frac{\partial \Phi}{\partial y}$$

Since this equation is symmetric, it admits reverse flow solutions as well. Thus, a solution utilizing central differences for transonic flow over a symmetric airfoil may admit two shocks, one of which would be a non-physical expansion one. Only when backward differences are used for supersonic points will the solution be limited to compression shocks. It can be shown that the use of backward differences in the

supersonic region introduces a viscous-like term similar to the right-hand side term in the full Navier-Stokes equations [1]. This "artificial viscosity" is a necessary ingredient in all transonic flow calculations.

A novel approach suggested by Hafez et al [22] to introduce the necessary artificial viscosity has been termed the Artificial Compressibility Method (ACM). Here, the artificial viscosity is introduced via the density, and equation (1.7) is rewritten as follows:

$$\frac{\partial}{\partial x}\left(\frac{1}{\tilde{\rho}}\frac{\partial \Psi}{\partial x}\right) + \frac{\partial}{\partial y}\left(\frac{1}{\tilde{\rho}}\frac{\partial \Psi}{\partial y}\right) = 0 \qquad (1.32)$$

were $\tilde{\rho}$ is the artificial density, given by:

$$\tilde{\rho} \approx \rho - \mu \rho_s \Delta s \qquad (1.33)$$

and

$$\rho_s \Delta s = (u/q)\,\rho_x \Delta x + (v/q)\,\rho_y \Delta y \qquad (1.34)$$

$$\mu = \max(0, 1 - 1/M_e^2,\ c(1 - 1/M_{e_{-1}}^2)), \qquad (1.35)$$

a switching function which vanishes in the subsonic region
(c is a factor ranging from 0 to 1)

This method allows the governing equation (1.32) to retain an elliptic form throughout the flowfield, and is currently in widespread use due to its ease of implementation [23], [24], [25].

1.5.2 Stability of the Iterative Scheme

In practice, the solution to the compressible flow problem, in delta form, involves a matrix system of the form:

$$[A]\{\delta\Psi\} = \{R\} \qquad (1.36)$$

The matrix [A] is usually taken to be the incompressible operator $(\partial_{xx} + \partial_{yy})$. This procedure will not converge for transonic flows, however, since a Laplacian

operator is not a sufficient approximation to the mixed-type governing operator. Results may only be obtained if the supersonic region is small and/or the artificial viscosity is greatly enhanced. Even in this instance, convergence problems will emerge if the computational grid is refined.

We wish to construct an iterative scheme that is based on the physical unsteady process with the inclusion of transient stabilizing terms which vanish when steady state has been reached. Consider the following form of the unsteady transonic equation of one-dimensional flow:

$$\gamma G_u + 2 u \alpha G_{xt} = (a^2 - u^2) G_{xx} \qquad (1.37)$$

It can be shown [13] that for equation (1.37) to represent a well-posed problem for supersonic flows, the coefficient of the G_{xt} term must be positive and larger than $\sqrt{1 - 1/M^2}$. Therefore, addition of a G_{xt} to an iterative scheme or enhancing it, if it already exists, means the addition to the iterative matrix terms such as:

$$\Delta x \frac{\partial}{\partial x}(G_t) = \Delta x \Delta t \frac{\partial}{\partial x}(\delta G) = (\delta G_l^{n+1} - \delta G_{l-1}^{n+1}) \qquad (1.38)$$

It should be mentioned that only VLSOR, marching with the flow, has a natural G_{xt} term in it. Other schemes such as point Jacobi, HLSOR, Zebroid, ADI, etc., do not have a G_{xt} term in them, thus it must be added explicitly.

1.6 Iterative Techniques for Transonic Flows

The finite element discretization of the governing partial differential equations results in a matrix system of the form:

$$[K]\{\Psi\} = \{f\} \qquad (1.39)$$

where [K] is a banded, symmetric matrix

{Ψ} is the vector of unknowns

{f} is the forcing function.

The matrix [K] is a function of the density and therefore it lags behind the stream function solution by one iteration. Convergence is attained when the L-2 norm (R_{L-2}) has reached a specified value, say of 10^{-8}, where

$$R_{L-2} = \sqrt{\sum_{i=1}^{n} R_i^2} \qquad (1.40)$$

1.6.1 Line Implicit Methods

(A) Vertical Line Successive Over-Relaxation (VLSOR) Method

VLSOR is a line-implicit method in which the solution at one vertical column of nodes is obtained using the most recent solution at the previous line and the previous solution at the next line as boundary conditions. The method proceeds by marching downstream in the direction of the flow. The resulting matrix system is tridiagonal, and the solution change, $\delta\Psi$ is over-relaxed by a factor ranging from 1 to 2 as follows:

$$[K]\,[\delta\Psi_i^{n+1}] = -\{R(\delta\Psi_{i-1}^{n+1}, \Psi_{i+1}^{n})\} \qquad (1.41)$$

The transient Ψ_{xt} term, as discussed previously, is inherent in the scheme, leading to a stable convergence.

(B) Zebroid Method

This method is essentially a horizontal line over-relaxation. Applied to each line, however, it produces a Ψ_{xt} term of varying sign, depending on the local flow direction. To prevent this, the scheme is applied to alternate lines and thus two horizontal sweeps are required to complete an iteration. A Ψ_{xt} must be explicitly added to ensure stability. More will be said about this method in Chapter 2, as it is one of the main focal points of this Thesis.

1.6.2 Field Solvers

(A) First and Second Degree Implicit Methods

These methods can be written, in the case for the stream function, as:

$$\epsilon [L] \delta^2 \Psi + \alpha [L] \delta \Psi = -\beta \{ [K] \{ \Psi \} - \{ f \} \} \qquad (1.43)$$

where $\epsilon = 0,1$ for first (Ψ_t) or second (Ψ_{tt}) methods respectively and α, β are acceleration factors. [L] is an operator approximating the compressible flow one. Once again, a Ψ_{xt} term is needed for stabiliity. An asymmetric operator [A] can be constructed for the supersonic region as [A] = [L] [T], where [T] is an element transformation matrix zeroing out the contribution at a supersonic point from downstream nodes within an element while doubling the contribution to that node from the upstream nodes in the element [26]. Figure 1.3 illustrates this procedure.

1.7 Scope of Thesis

This Thesis addresses some aspects of the stream function solution of transonic flow problems.

The problem of the double-valuedness of mass flux vs Mach number is investigated by three different approaches. It is applied to internal flow problems.

A finite element version of the horizontal line relaxation algorithm (Zebroid) is developed in order to accelerate the convergence rate of the iterative process.

Results from external and internal flow geometries are presented in each and discusssed in each chapter.

CHAPTER 2

THE ZEBROID ALGORITHM APPLIED TO THE STREAM FUNCTION EQUATION

In this chapter, a horizontal line-implicit relaxation (Zebroid) method to solve the transonic flowfield is presented. This scheme has a faster convergence rate than VLSOR methods since solving the flow in a direction parallel, rather than perpendicular to, the flow direction results in flow information being spread more rapidly throughout the field, especially in the presence of discontinuities. The Zebroid scheme is even shown to converge faster than implicit ones.

2.1 Description of Zebroid Algorithm

The Zebroid algorithm is a horizontal line relaxation in which only every second line is updated during one sweep. Thus, one iterative step requires two field sweeps, termed the "odd" and "even" sweeps. This two-step procedure is necessary, otherwise a transient Ψ_{xt} would appear in the governing equations, causing convergence difficulties at high Mach numbers. During each sweep a Ψ_{xt} term must therefore be added explicitly, to help the convergence of transonic calculations. Figure 2.1 demonstrates this method for isolated airfoils. Here, the "odd" sweep is performed first, starting at the airfoil and moving outward towards the far-field boundary. At the first station, only one row of elements is assembled, since there are no elements below the airfoil. All other stations include two rows of elements, above and below the row of unknown nodes. In the diagram, the term "dynamic boundary conditions" refers to values which are kept constant only during the solution at one particular station.

In Figure 2.2, the application of the method to a compressor cascade is shown. In this instance, the direction of sweep is reversed during one iterative step to

allow for a more rapid exchange of flow information between the suction and pressure surfaces of the airfoil.

A distinctive feature of the Zebroid algorithm is brought out here. In other solvers, the periodicity condition is maintained only between two lines, such as AB and EF, shown in the same figure. While this guarantees periodicity in Ψ, it only imposes velocity periodicity in a mean sense. The implementation of a Zebroid solver necessitates the use of an additional row of elements above EFGH and another one below ABCD. Therefore, periodicity in Ψ can be imposed between three lines centered on EFGH and ABCD, guaranteeing periodicity in velocity.

2.2 Boundary Conditions

As stated in Section 1.5, the governing equation to be solved for is:

$$\frac{\partial}{\partial x}\left(\frac{1}{\tilde{\rho}}\frac{\partial \Psi}{\partial x}\right) + \frac{\partial}{\partial y}\left(\frac{1}{\tilde{\rho}}\frac{\partial \Psi}{\partial y}\right) = 0$$

where:

$$\tilde{\rho} = \rho - \mu \frac{\partial \rho}{\partial s}\Delta s$$

$$\approx \rho - \mu(\rho_e - \rho_{e-1})$$

and $\mu = \max(0, 1 - 1/M_e^2, c(1 - 1/M_e^2))$.

The boundary conditions are stated below for isolated airfoils and cascades.

2.2.1 Isolated Airfoils

Figure 2.3 illustrates the boundary conditions for flow over an isolated, symmetric airfoil. They are:

on AB : $\Psi = 0$

on DC : $\Psi = 1$

on DA and CB : Ψ varies linearly.

2.2.2 Compressor Cascades

The second part of Figure 2.3 shows the boundary conditions for flow through a compressor cascade. They are:

on BC : $\Psi = 0$ (blade suction surface)

on GF : $\Psi = 1$ (blade pressure surface)

on inlet and exit : Ψ is unknown, and a contour integral is evaluated as

$$\frac{1}{\rho}\int N_i \frac{\partial \Psi}{\partial n} ds$$

In addition, flow periodicity is maintained between AB and HG, as well as between CD and FE. One should note that the contour integrals cancel one another on such periodicity lines.

2.3 Numerical Results

The Zebroid algorithm is applied to the solution of subcritical and supercritical flows flows over a NACA 0012 symmetric airfoil. Figure 2.4a shows the results of the computations at various free-stream Mach numbers from subcritical to supersonic. Flows at Mach numbers higher than 0.8 were evaluated by alternating the solution of the stream function equation with the integration of the first order vorticity definition equation (1.10), at each iteration. The grid used consisted of 1008 nodes, with 31 points on the airfoil and 15 subdivisions across the field.

In Figure 2.4b, the application of the method to a cascade of multiple circular arc (MCA) airfoils at $M_\infty = 0.76$ is shown. The shock on the suction surface is sharp

and well defined. To demonstrate the accuracy of the method, the results over an isolated NACA 0012 at M_∞= 0.80 and 0.85 are compared with a reference velocity potential solution in Figures 2.4c and 2.4d. The grid used for the MCA solution employed 855 nodes and is shown in Figure 2.5.

Finally, the rates of convergence of various iterative techniques for flow over an isolated NACA 0012 at M_∞= 0.85 are compared in Figure 2.6. The Zebroid method is shown to be faster than VLSOR and even the implicit methods. The scheme is particularly attractive when one considers that each individual iteration is also more computationally efficient since the matrix system is tridiagonal, compared to the larger global matrices used in implicit methods and their associated core requirements.

CHAPTER 3

THE STREAM FUNCTION AND SECOND ORDER VORTICITY EQUATION ALGORITHM

As demonstrated in the previous chapter, successful results can be obtained for transonic flows over isolated airfoils using the stream function equation in conjunction with the first-order vorticity equation. In this instance, the solution started from the far-field boundary, at which the flow velocity is known. A problem arises, however, if this approach is applied to a cascade where the flow at the airfoil surface is unknown and especially for choked cascades in which a shock may extend across the full width of the channel and an initial data line along which the solution is known does not exist.

One therefore must strive to construct a scheme in which an initial data line is not required. This chapter introduces a second order formulation for the flow velocity, q, whereby we turn the vorticity equation into a field one in order to overcome the double-valuedness problem. This new method is first applied to isolated airfoils, so that its applicability to more complicated cases such as cascades can be justified.

3.1 Description of Algorithm

Let us reconsider the first-order vorticity equation:

$$\frac{\partial u}{\partial y} - \frac{\partial v}{\partial x} = 0 \tag{3.1}$$

Defining:

$$\alpha = \frac{u}{q} = \cos\theta \tag{3.2a}$$

$$-\beta = \frac{v}{q} = \sin\theta \tag{3.2b}$$

Then (3.1) can be rewritten as:

$$\frac{\partial}{\partial y}(q\alpha) + \frac{\partial}{\partial x}(q\beta) = 0 \tag{3.3}$$

or

$$\left[\frac{\partial \alpha}{\partial y} + \frac{\partial \beta}{\partial x}\right]\{q\} = 0 \tag{3.4}$$

Multiplying by the following operator in order to make the equation second-order:

$$\left[-\alpha\frac{\partial}{\partial y} - \beta\frac{\partial}{\partial x}\right]\left[\frac{\partial \alpha}{\partial y} + \frac{\partial \beta}{\partial x}\right]\{q\} = 0 \tag{3.5}$$

Expanding:

$$\beta\frac{\partial^2}{\partial x^2}(\beta q) + \alpha\frac{\partial^2}{\partial y^2}(\alpha q) + \alpha\frac{\partial^2}{\partial y \partial x}(\beta q) + \beta\frac{\partial^2}{\partial x \partial y}(\alpha q) = 0 \tag{3.6}$$

This can be expressed as:

$$Aq_{xx} + 2Bq_{xy} + Cq_{yy} = D \tag{3.7}$$

where

$$A = \beta^2$$

$$B = \alpha\beta$$

$$C = \alpha^2$$

The classification of this PDE is found by evaluating $(B^2 - AC)$ as:

$$(B^2 - AC) = \alpha^2\beta^2 - \alpha^2\beta^2 = 0$$

thus the equation is parabolic.

By treating the problem as a field one, we eliminate the need for an initial data line. The Galerkin finite element discretization multiplies equation (3.6) by the shape function, followed by integration by parts, yielding the following:

$$\iint \left\{ (N_i\beta)_x (q\beta)_x + (N_i\alpha)_y (q\alpha)_y + (N_i\alpha)_y (q\beta)_x + (N_i\beta)_x (q\alpha)_y \right\} dxdy$$

$$- \int \left\{ N_i\beta (q\beta)_x dy + N_i\alpha (q\alpha)_y dx + N_i\alpha (q\beta)_x dx + N_i\beta (q\alpha)_y dy \right\} = 0 \tag{3.8}$$

The contour integral term can be rewritten as:

$$-\int N_i \left[\beta (q\beta)_x + \beta (q\alpha)_y\right] dy + N_i \left[\alpha (q\alpha)_y + \alpha (q\beta)_x\right] dx \qquad (3.9)$$

$= 0$ on all boundaries where q is not specified, since the first-order vorticity equation is identically satisfied.

$= 0$ on all boundaries where q is specified, since $N_i = 0$.

Thus, the boundary conditions are satisfied by ignoring the contour integral. This of course presents great advantages on airfoils and on cascades blades. One note that the value of q must be specified at least at one point of the flow.

The finite element integral to be evaluated is hence given by:

$$\iint \{(N_i\beta)_x (q\beta)_x + (N_i\alpha)_y (q\alpha)_y + (N_i\alpha)_y (q\beta)_x + (N_i\beta)_x (q\alpha)_y\} dxdy = 0 \qquad (3.10)$$

The flow angles β and α are known from the solution of the stream function equation. The overall procedure for this scheme is shown on the flow chart of Figure 3.1.

3.2 Boundary Conditions for Isolated Airfoils

A C-grid of the type shown in Figure 3.2 is used to discretize the domain. The appropriate boundary conditions for an isolated airfoil are:

Ψ equation (eq. (1.7))

on AB and BC : $\Psi = u_\infty y$ (3.11a)

on AC : $\Psi = u_\infty y$ (3.11b)

on airfoil surface : $\Psi = 0$ (3.11c)

q equation (eq. (3.5))

on AB and BC : $q = u_\infty$ (3.12a)

on AC : q = unknown, natural b.c. satisfied (3.12b)

on airfoil surface : q = unknown, natural b.c. satisfied (3.12c)

3.3 Numerical Results

Following the steps of the algorithm shown in Figure 3.1 results for the flow over an isolated NACA 0012 airfoil are obtained. The flow angles α and β are first evaluated at the nodes knowing the stream function distribution. Equation (3.10) is subsequently applied to calculate q using an implicit method in which the global boundary conditions for q are used to "drive" the solution.

Unfortunately, the proposed method has proven to be ineffective for the problem at hand. The results obtained indicate a Mach number distribution that is too low and displaced significantly downstream compared to reference test cases, even for purely subsonic flow. With some effort, the cause for this behaviour became apparent. In section 3.1, the nature of the governing equation for q was determined to be parabolic and a different solution was deemed necessary and a line implicit approach is adopted. Starting at the outermost line of elements defining the "C" in the grid, the solution is advanced by marching inwards, assembling only one row of elements at a time. While marching in the general flow direction, the most recent values of q at the preceeding nodes are utilized. This process is nothing but a horizontal line successive overrelaxation (HLSOR) scheme applied to a C-grid.

In this instance, preliminary results for subsonic (M_∞= 0.72) flow over the NACA 0012 show good correlation with the reference stream function case (Figure 3.3).

Further work was not carried out after this stage, since this HLSOR method as applied to the second order equation contains no advantages compared to the first order vorticity equation.

CHAPTER 4

THE STREAM FUNCTION AND PRESSURE EQUATION ALGORITHM

The first order vorticity scheme, although successful for transonic flows over isolated airfoils and unchoked cascades, cannot be applied to choked cascades. The second order method presented in Chapter 3 seemed to provide a compromise but was shown to be restricted in its applicability and presents no particular advantages.

In this chapter, a third approach is undertaken for the same problem, whereby the stream function equation is solved in conjunction with a pressure equation. Knowing the flow velocities from the stream function field, as well as the pressures, an energy equation is used to determine the value of density.

4.1 Description of Algorithm

Let us consider the two-dimensional form of the Euler equations for steady, inviscid flow in the absence of body forces:

$$\rho u u_x + \rho v u_y = - p_x \tag{4.1a}$$

$$\rho u v_x + \rho v v_y = - p_y \tag{4.1b}$$

Recalling the definition of the stream function, Ψ:

$$u = \frac{1}{\rho}\frac{\partial \Psi}{\partial y} \quad , \quad v = -\frac{1}{\rho}\frac{\partial \Psi}{\partial x} \tag{4.2}$$

Using these, equations (4.1a) and (4.1b) can be rewritten as:

$$p_x + f = 0 \tag{4.3a}$$

$$p_y + g = 0 \tag{4.3b}$$

where $f = \Psi_y u_x - \Psi_x u_y$

$g = \Psi_y v_x - \Psi_x v_y$

Adding the x-derivative of the x-momentum equation to the y-derivative of the y-momentum equation and applying the Method of Weighted Residuals to the resulting Poisson equation yields:

$$\iint W\,((p_x + f)_x + (p_y + g)_y)\,dA = 0 \qquad (4.4)$$

Upon integration by parts, we obtain:

$$\iint (W_x\,(p_x + f) + W_y\,(p_y + g))\,dA = \int W\,((p_x + f)\,dy - (p_y + g)\,dx) \qquad (4.5)$$

Equation (4.5) is used to evaluate the pressure distribution once the Ψ field has been established. Subsequently, the density is obtained from the conservation of enthalpy relationship:

$$H_o = \text{CONSTANT} = C_p T_o \qquad (4.6)$$

or, for an ideal gas;

$$H_o = \left(\frac{\gamma}{\gamma - 1}\right)\left(\frac{p}{\rho}\right) + \frac{u^2 + v^2}{2} = \text{CONSTANT} \qquad (4.7)$$

Since the enthalply is constant in the far-field, the density at an arbitrary point is determined from equation (4.7), i.e., $H_o = H_\infty = \text{CONSTANT}$.

The overall procedure for this scheme is shown on the flowchart of Figure 4.1.

4.2 Boundary Conditions for Isolated Airfoils

Once again, a C-grid of the type illustrated in Figure 3.2 is employed. The boundary conditions for Ψ are identical to those stated in section 3.2. The pressure boundary conditions are as follows:

on AB and BC : $p = p_\infty$ (4.8a)

on AC : p = unknown, but contour integral vanishes (4.8b)

on airfoil : p = unknown, but contour integral vanishes (4.8c)

As in the second order q case, the contour integral in equation (4.5) vanishes even on boundaries where the pressure is unknown because the governing equation itself is identically satisfied.

4.3 Numerical Results

Mach number distributions obtained from the present method for the NACA 0012 are illustrated in Figures 4.2 and 4.3, for free-stream Mach numbers of 0.80 and 0.85 respectively. Plotted against them are the reference results from a velocity potential and an Euler equation solution. The correlation is seen to be good, verifying the applicability of the method. The only drawback of this scheme is in its relatively slow convergence rate when compared to, say, the velocity potential equation. This is due to the slow convergence of the pressure field. Research is currently underway to accelerate the solution.

Figure 4.4 compares the pressure coefficient distribution at Mach number 0.80 obtained with the present scheme with the experimental results given in ref. [27]. The shock is displaced downstream compared to the experimental data but the correlation is remarkable given that the analysis does not account for the boundary layer effect.

CHAPTER 5

CONCLUSIONS

This Thesis has addressed and solved some of the problems that complicate the use of the stream function approach for the solution of inviscid transonic flow problems. A finite element line-implicit computational algorithm has been developed which reduces the number of iterations required for convergence of the nonlinear problem. The algorithm proves particularly appropriate for cascade problems. It has also subsequently found applications in other approaches such as the velocity potential.

Secondly, three distinct methods of tackling the double-valuedness of mass flux for transonic flows have been proposed with two of them successfully applied to the solution of external and internal flow problems.

REFERENCES

[1] Murman, E.M. and J.D. Cole, "Calculation of Plane Steady Transonic Flows," AIAA Journal, Vol. 9, 1971, pp. 114-121.

[2] Murman, E.M., "Analysis of Embedded Shock Waves Calculated by Relaxation Methods," AIAA Journal, Vol. 12, No. 5, 1974, pp. 626-632.

[3] Newman, P.A. and J.C. South, "Influence of Nonconservative Differencing on Transonic Streamline Shapes," AIAA Journal, Vol. 14, No. 8, 1976, pp. 1148-1149.

[4] Pearcy, H. H., "The Aerodynamic Design of Section Shapes for Swept Wings," Advances in Aeronautical Sciences, Vol. 3, Pergamon Press, 1962.

[5] Whitcomb, R.T. and R. Clark, "An Airfoil Shape for Efficient Flight at Supercritical Mach Numbers," NASA TM X-1109, 1965.

[6] Bauer, F. et al., "Supercritical Wing Sections," Lecture Notes in Economics and Mathematical Systems, Vol. 66, Springer-Verlag, 1972.

[7] Jameson, A., "Numerical Calculation of Three Dimensional Transonic Flow Over a Yawed Wing," Proc. AIAA Computational Fluid Dynamics Conf., Palm Springs, Calif., pp. 18-26, July 1973.

[8] Steger, J.L. and H. Lomax, "Transonic Flow About Two-Dimensional Airfoils by Relaxation Procedures," AIAA Journal, Vol. 10, No. 1, 1972, pp. 49-54.

[9] Bailey, F.R. and J.L. Steger, "Relaxation Techniques for Three-Dimensional Transonic Flows About Wings," AIAA Paper 72-189, Jan. 1972.

[10] South, J.C. and A. Brandt, "Application of a Multi-Level Grid Method to Transonic Flow Calculations," **Transonic Flow Problems in Turbomachinery**, (ed. T.C. Adamson), Hemisphere Publ. Corp., 1977, pp. 180-208.

[11] Ballhaus, W.F. et al., "Implicit Approximate Factorization Schemes for the Efficient Solution of Steady Transonic Flow Problems," Proc. 3rd AIAA Computional Fluid Dynamics Conf., Albuquerque, N.M., June 1977, pp. 27-34.

[12] Eberle, A. "Eine Method Finiter Elements Berechnungder Transsonicken Potential-Strimung un Profile," MBB 1352 (0), 1977.

[13] Hafez, M. et al., "Artificial Compressibility Method for Numerical Solutions of Transonic Full Potential Equation," AIAA Journal, Vol. 17, No. 8, 1979, pp. 834-844.

[14] Holst, T.L. and W.F. Ballhaus, "Fast Conservative Schemes for the Full Potential Equation Applied to Transonic Flows," AIAA Journal, Vol. 17, No. 2, pp. 145-152, 1979.

[15] Purvis, J.W. and J.E. Burkhalter, "Prediction of Critical Mach Numbers for Store Configurations," AIAA Journal, Vol. 17, No. 11, 1979, pp. 1170-1177.

[16] Emmons, H.W., "The Numerical Solution of Compressible Fluid Flow Problems," NACA TN 932, 1944.

[17] Hafez, M.M. and D. Lovell, "Numerical Solution of Transonic Stream Function Equation," AIAA Journal, vol. 21, No. 3, 1983, pp. 327-335.

[18] Jameson, A., "Transonic Airfoil Calculations Using the Euler Equations," **Numerical Methods in Aeronautical Fluid Dynamics**, (ed. P.L. Roe), Academic Press, London, 1982, pp. 289-308.

[19] Habashi, W.G., "Potential Flows," Finite Element Method in Fluid Mechanics and Heat Transfer Course Notes, Concordia University-Pratt and Whitney Canada-Purdue University, 1983.

[20] Habashi, W.G. and M.M. Hafez, "Finite Element Stream Function Solutions of Transonic Rotational Internal and External Flows," Journal of Numerical Methods for Partial Differential Equations, Vol. 1, No. 2, 1985, pp. 127-144.

[21] Burden, R.L., J.D. Faires and A.C. Reynolds, **Numerical Analysis**, Prindle, Weber & Schmidt, Boston, Mass., 1981.

[22] Hafez, M.M., J.C. South and E.M. Murman, "Artificial Compressibility Methods for Numerical Solutions of Transonic Full Potential Equation," AIAA Journal, Vol. 17, 1978, pp. 838-844.

[23] Habashi, W.G., E.G. Dueck and D.P. Kenny, "Finite Element Approach to Compressor Blade-to-Blade Cascade Analysis," AIAA Journal, Vol. 17, 1979, pp. 693-698.

[24] Deconinck, H. and Ch. Hirsch, "Finite Element Methods for Transonic Blade-to-Blade Calculation in Turbomachines," ASME Journal of Engineering for Power, Vol. 103, 1981, pp. 665-667.

[25] Habashi, W.G. and P.L. Kotiuga, "Numerical Solution of Subsonic and Transonic Cascade Flows," International Journal for Numerical Methods in Fluids, Vol. 2, 1982, pp. 317-330.

[26] Habashi, W.G., (Editor), **Advances in Computational Transonics**, Pineridge Press, Swansea, U.K., p. 680, 1985.

[27] Thibert, J.J., M. Grandjacques and L.H. Ohman, "NACA 0012 Airfoil," Experimental Database for Computer Program Assessment, AGARD Advisory Report, No. 138, 1979.

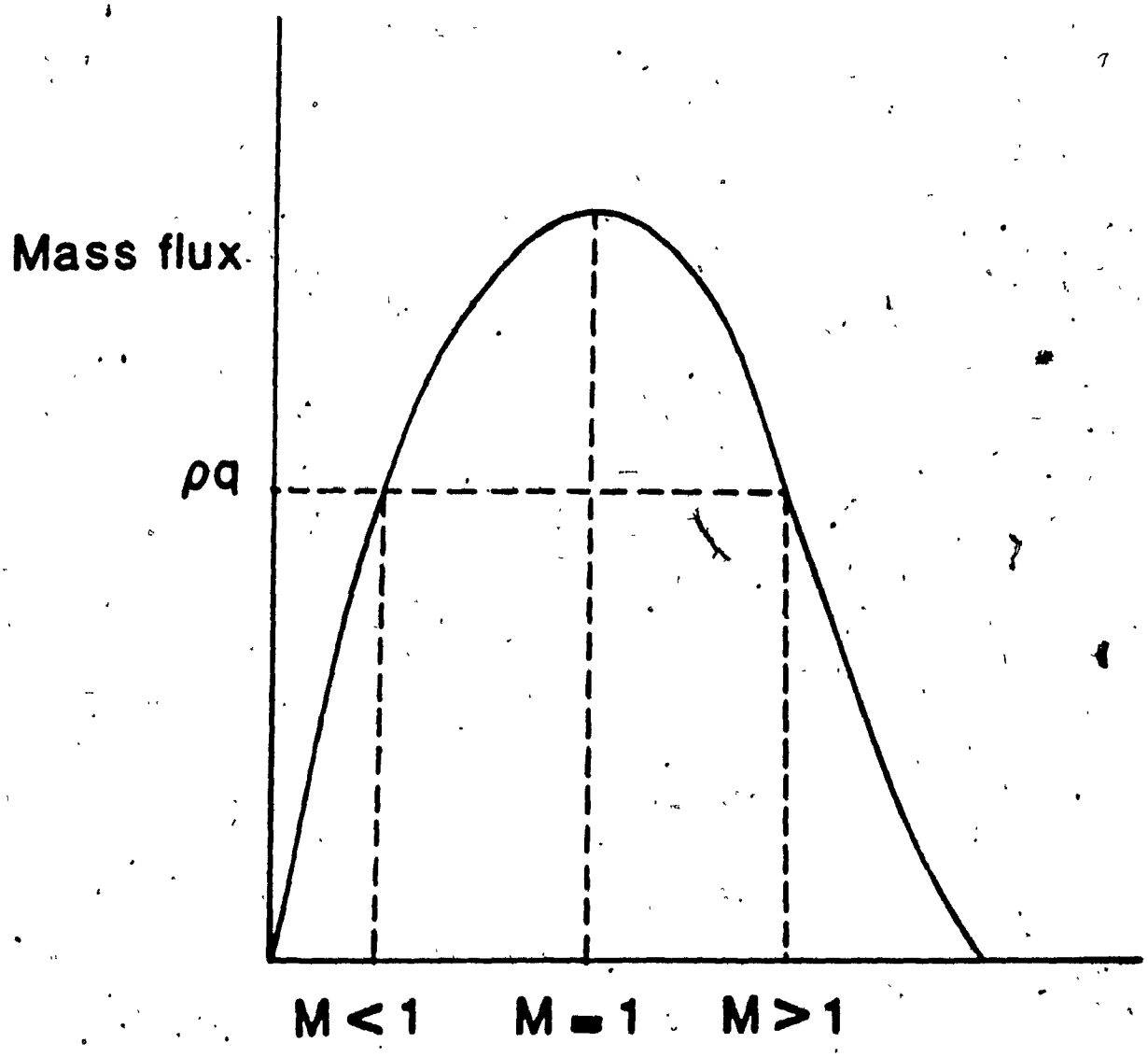

Fig. 1.1 Mass Flux vs. Mach Number

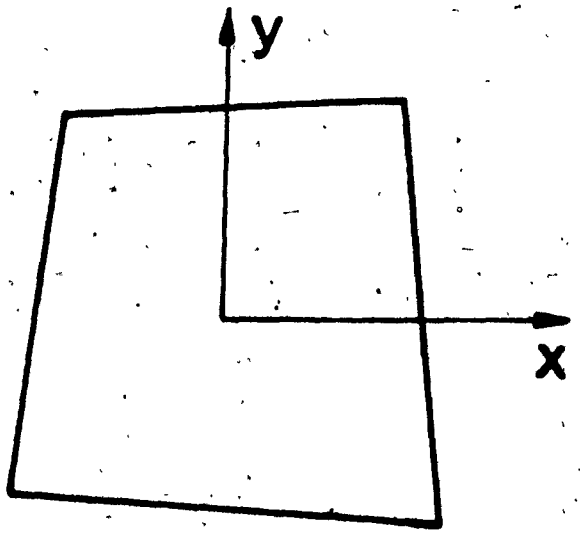

Actual element

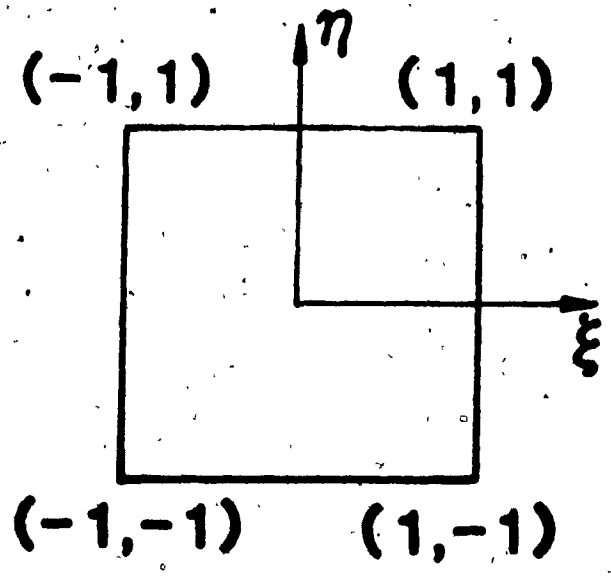

Undistorted element

Fig. 1.2 Actual and Parent Element

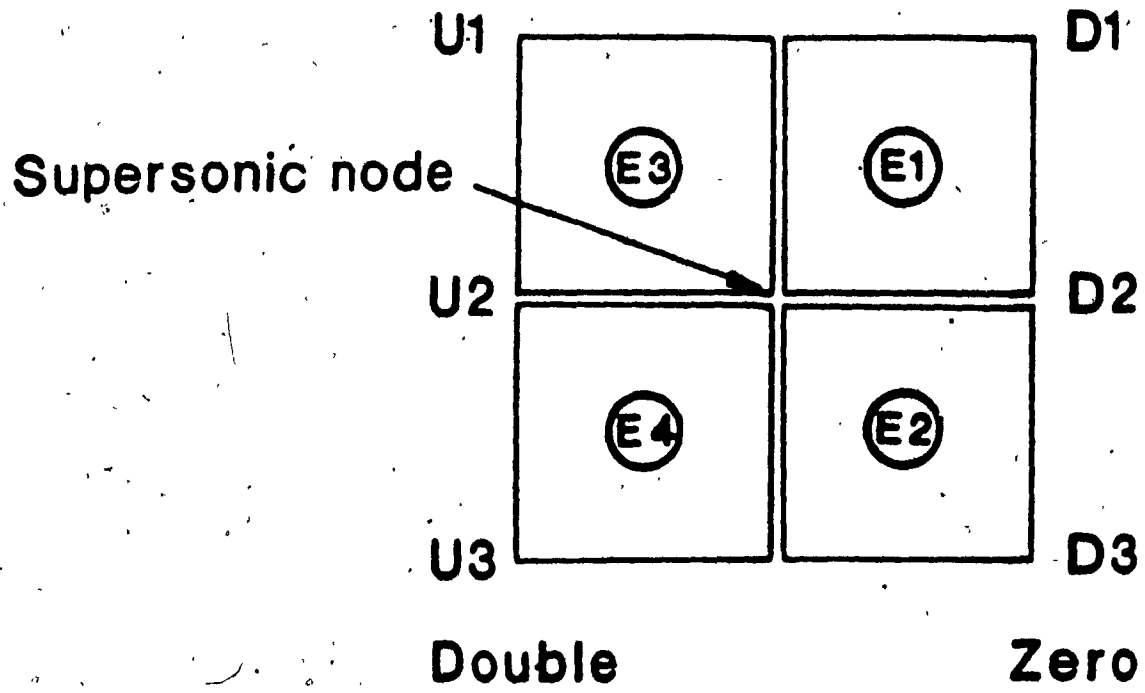

Fig. 1.3 Ψ_{xt} for a Field Solver

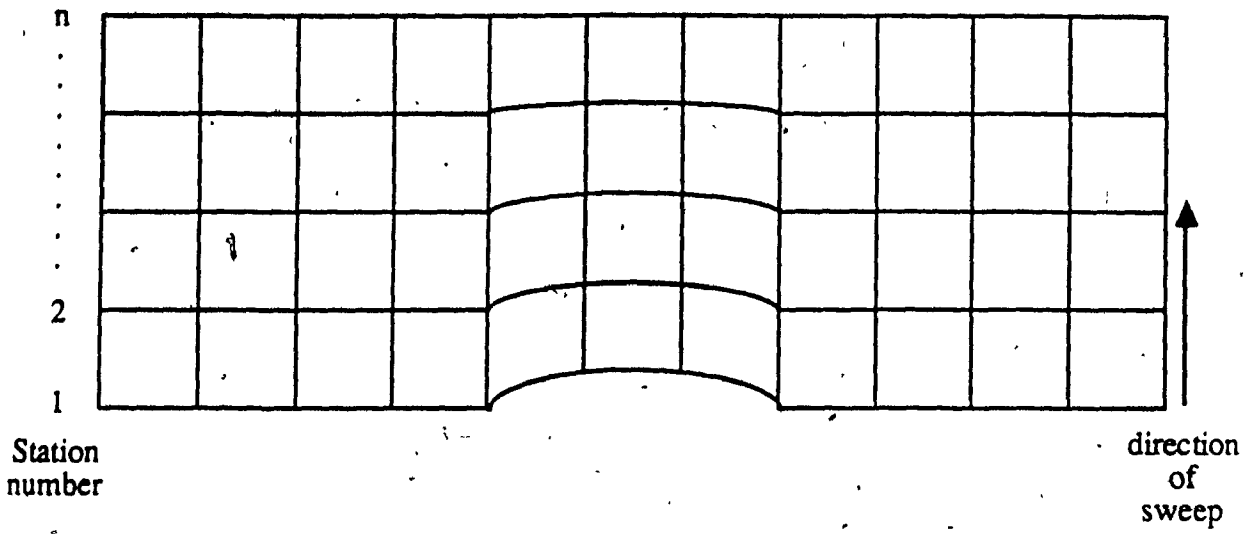

Station Types

(1) at airfoil

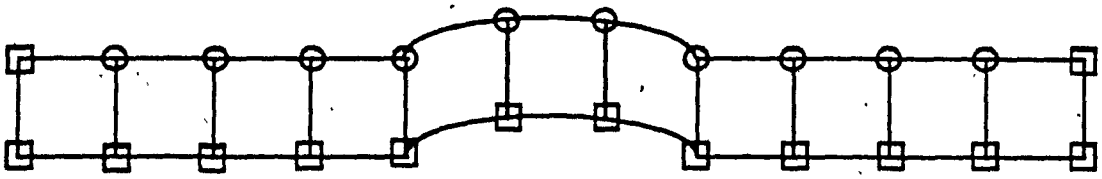

(2) all other stations

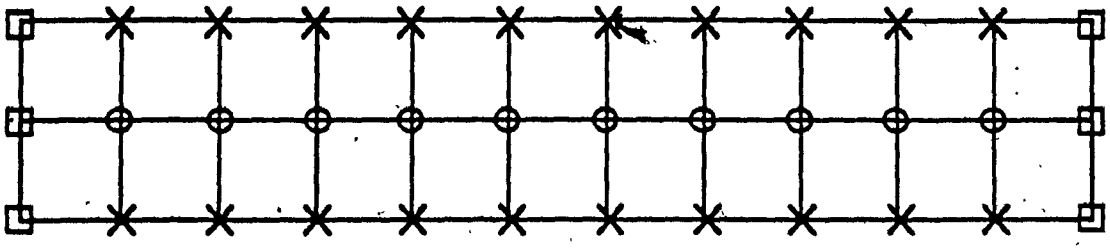

○ unknown value

× dynamic boundary condition

□ Dirichlet boundary condition

Fig. 2.1 Zebroid Method for Isolated Airfoils

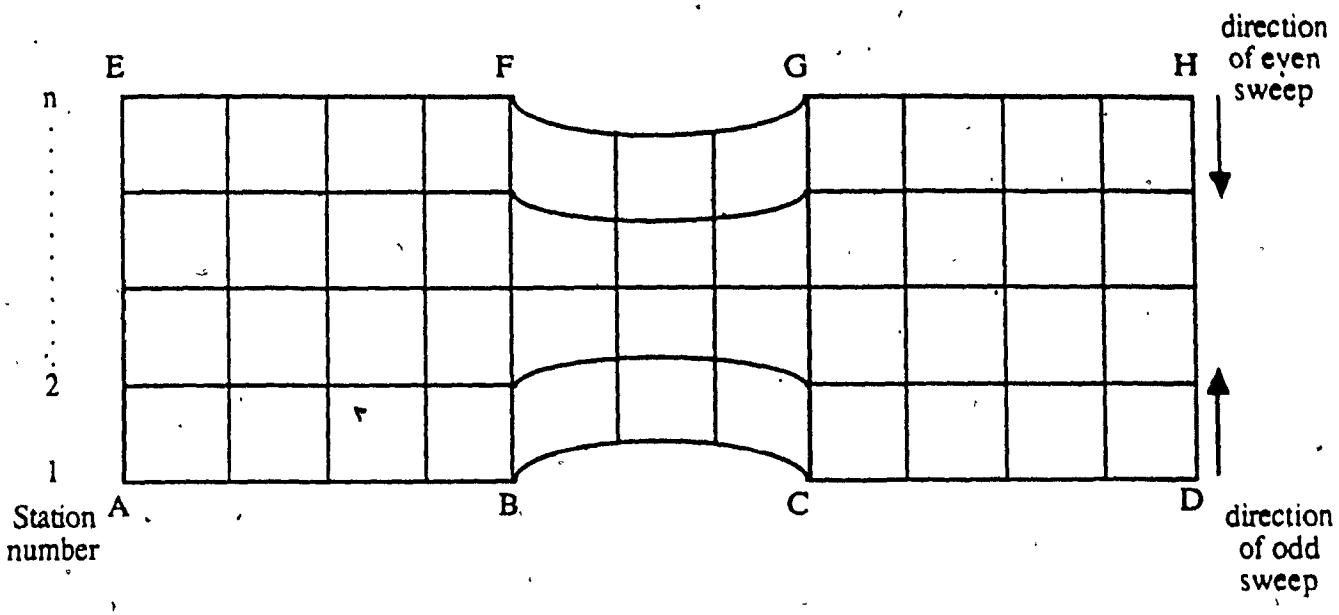

Station Types

(1) at airfoil

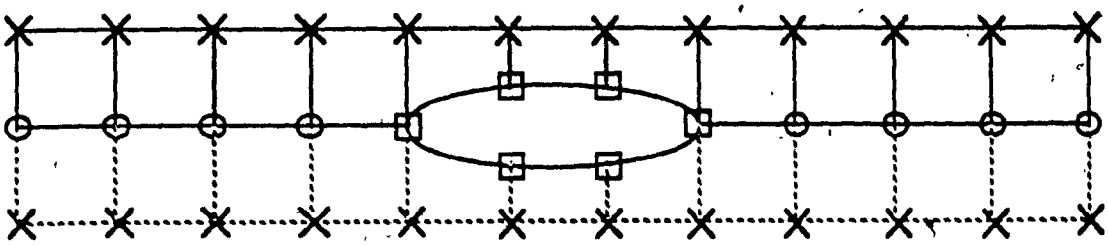

(2) all other stations

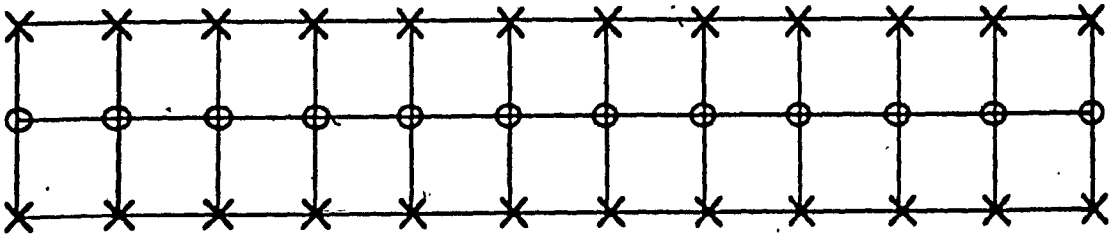

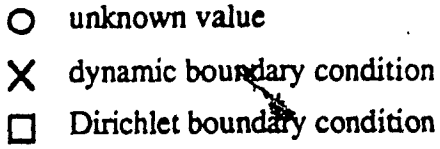

Fig. 2.2 Zebroid Method for Cascades

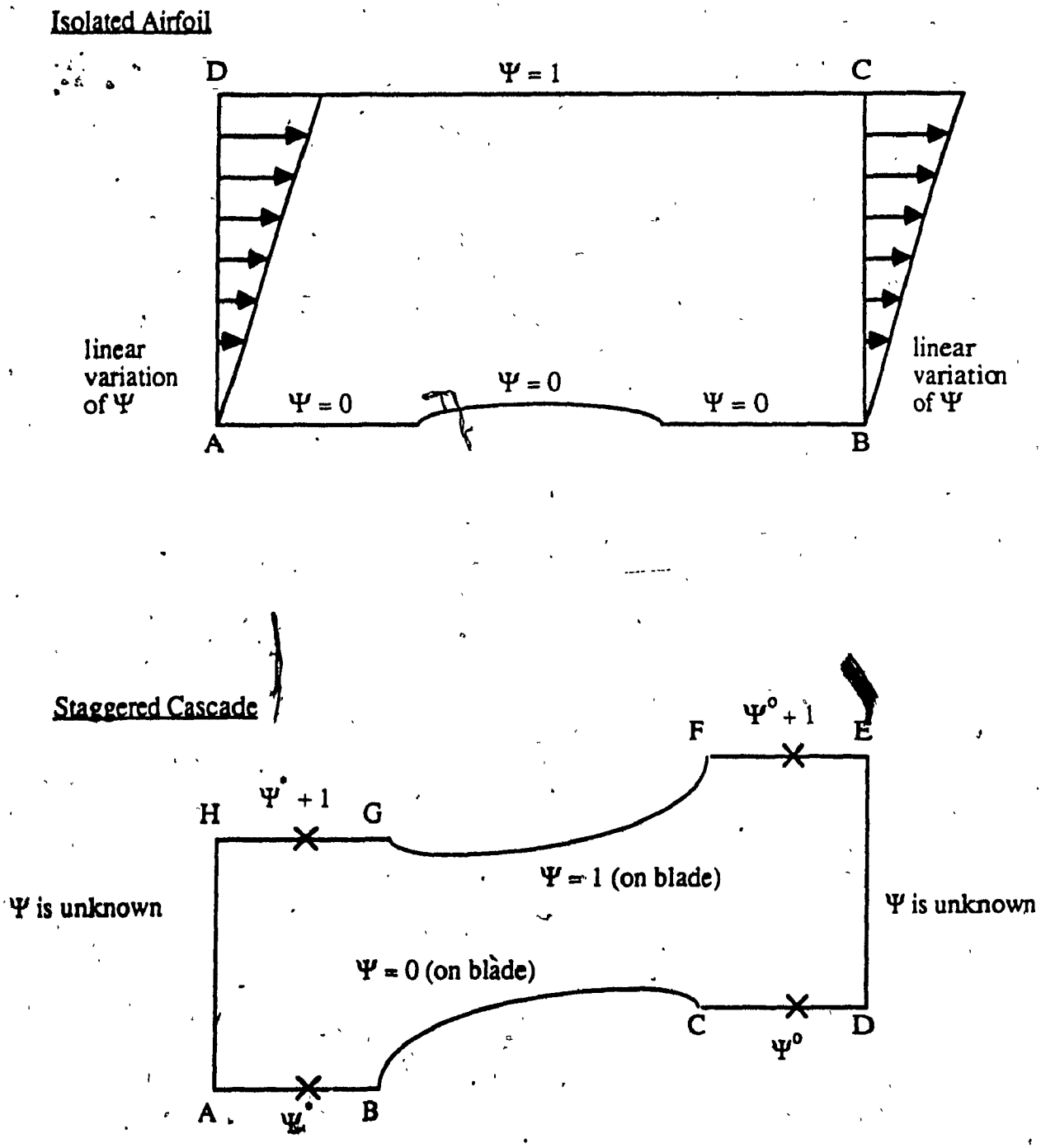

Fig. 2.3 Boundary Conditions for Stream Function

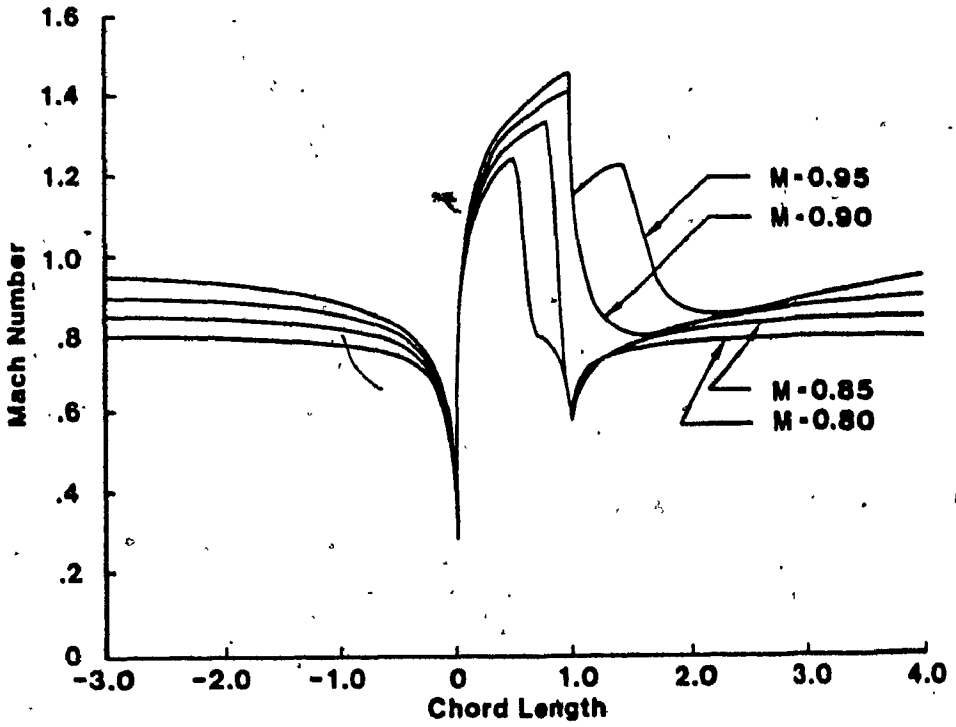

Fig. 2.4a Mach Number vs. Percent Chord for NACA 0012 Airfoil, Ψ Solution

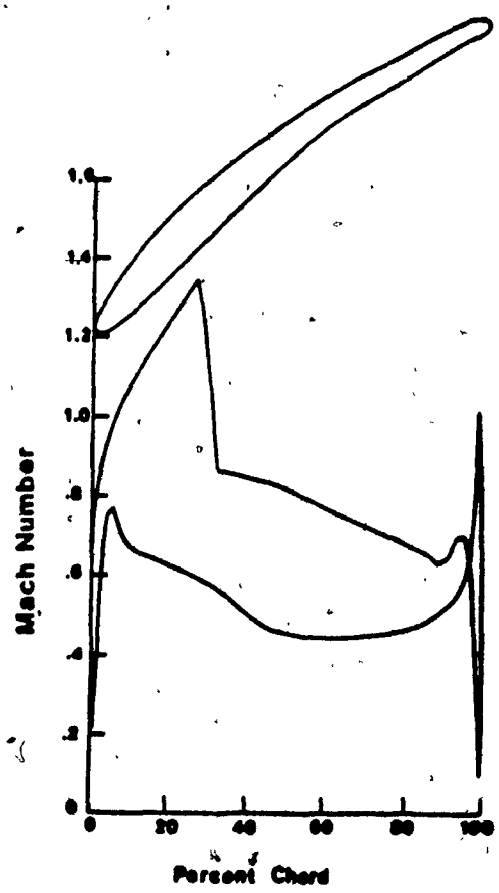

Fig. 2.4b Mach Number vs. Percent Chord for MCA Cascade, Ψ Solution, M_{∞}= 0.76

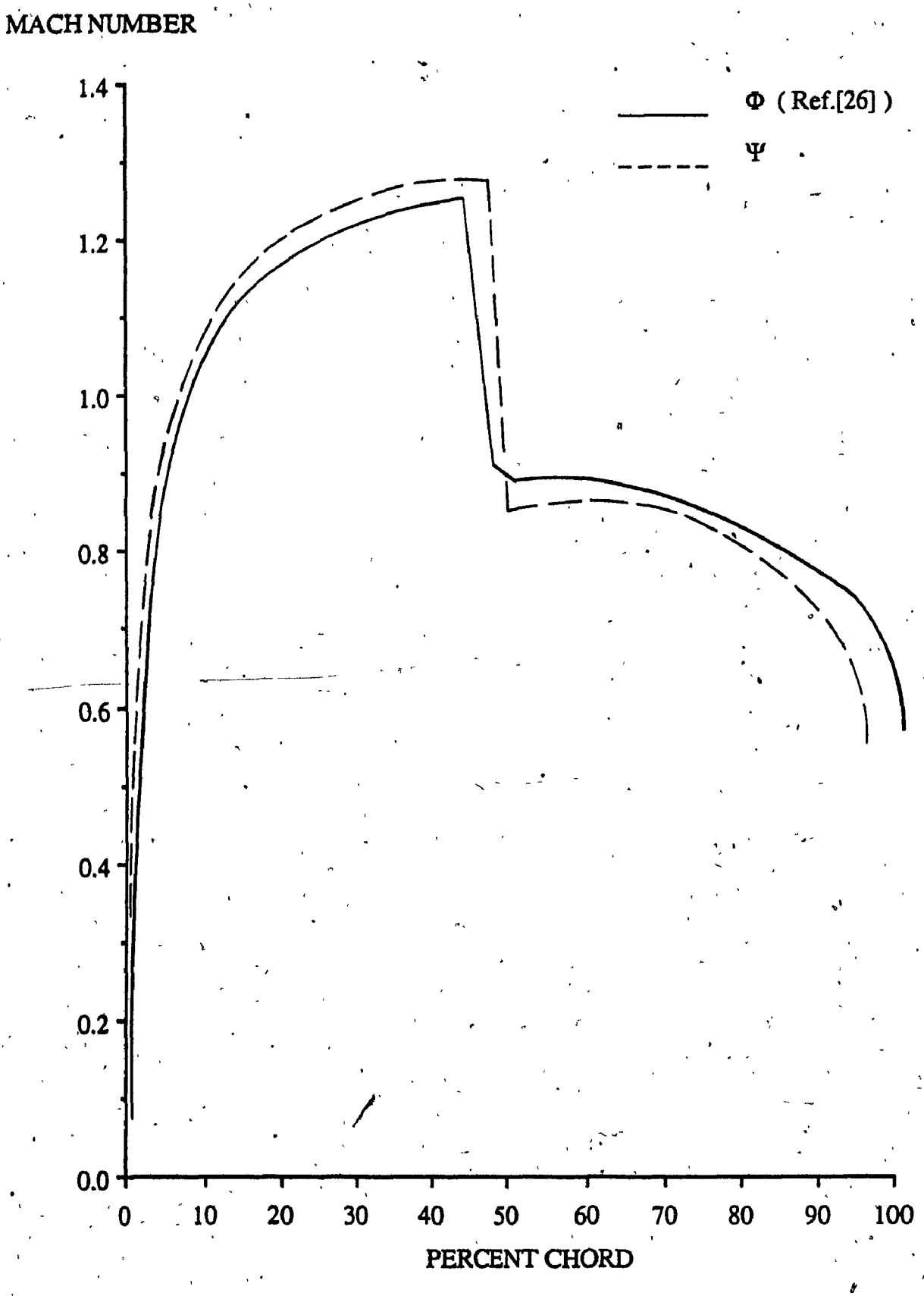

Fig. 2.4c **Mach Number vs. Percent Chord for NACA 0012 Airfoil, Ψ Solution, $M_\infty = 0.80$**

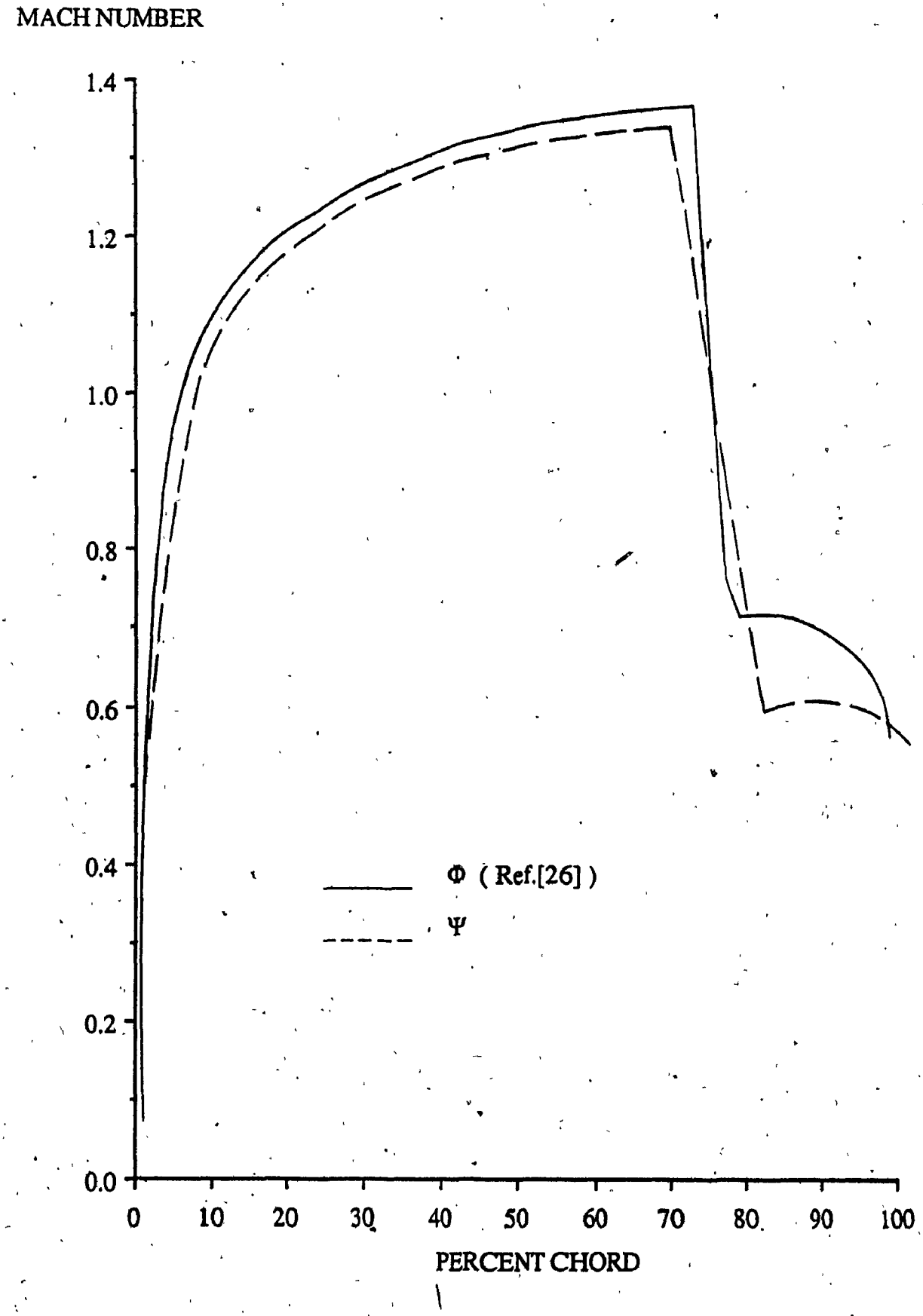

Fig. 2.4d **Mach Number vs. Percent Chord for NACA 0012 Airfoil, Ψ Solution, $M_\infty = 0.85$**

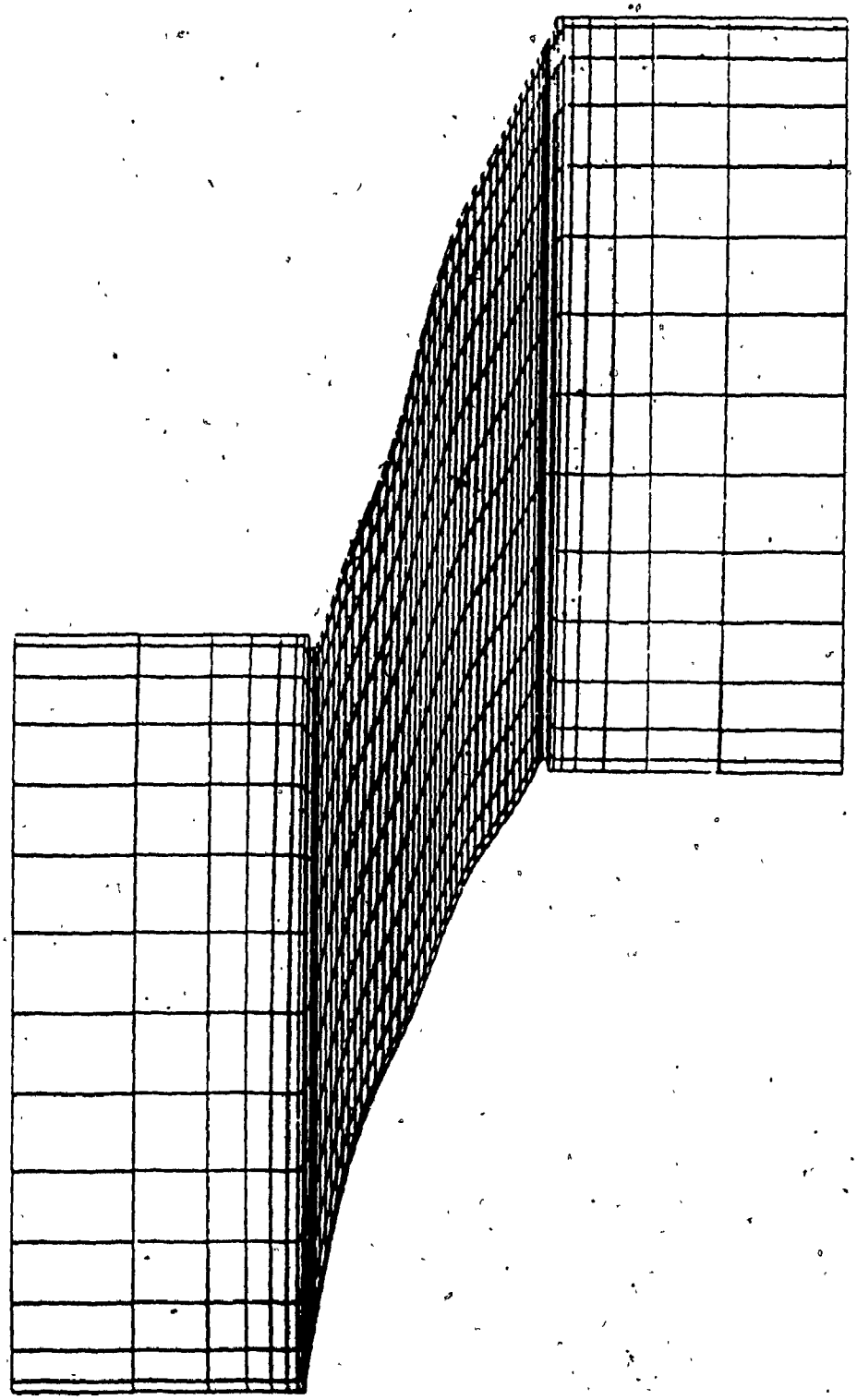

Fig. 2.5 Staggered MCA Cascade

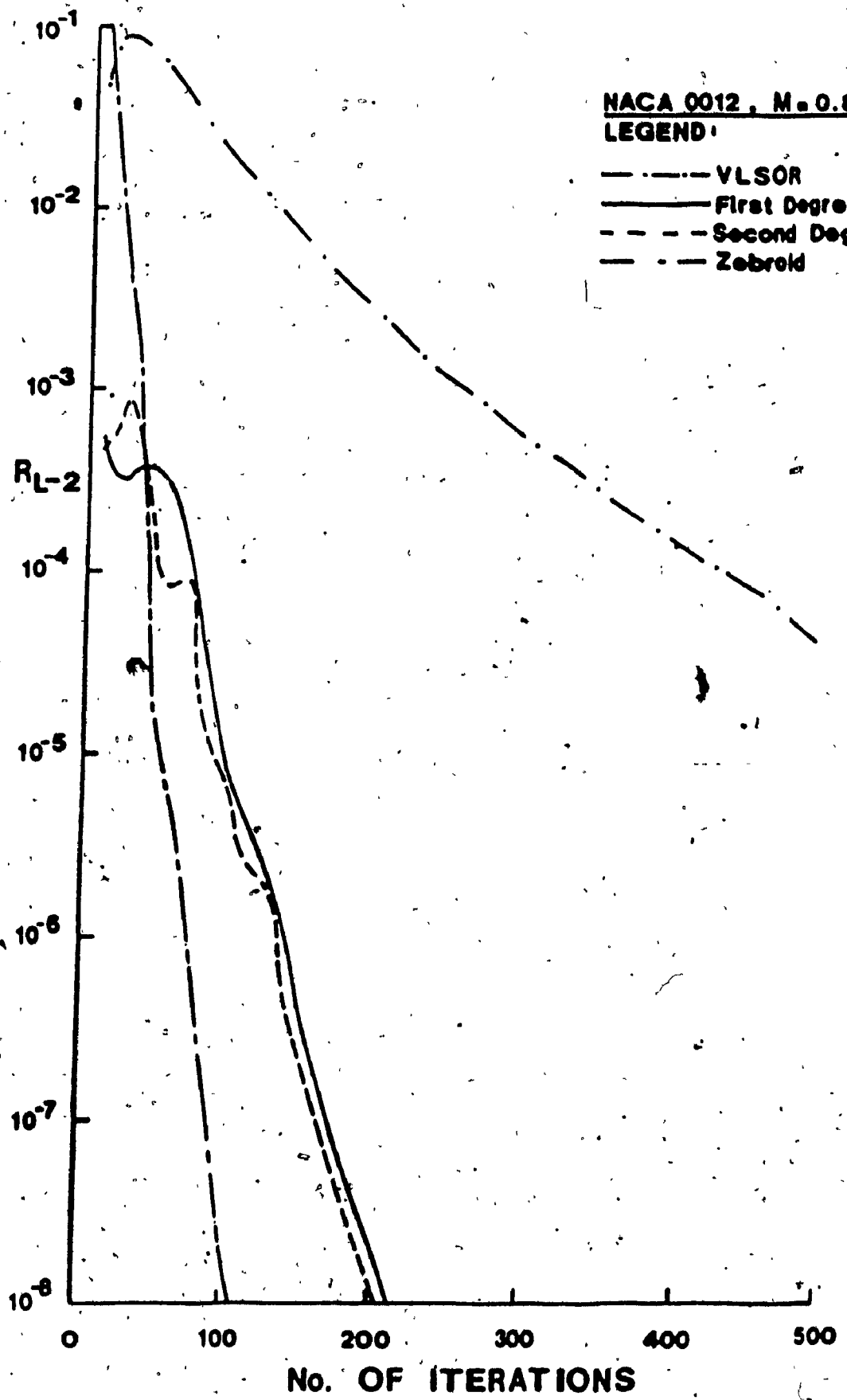

Fig. 2.6 Rates of Convergence of Various Solvers at $M_\infty = 0.85$, NACA 0012

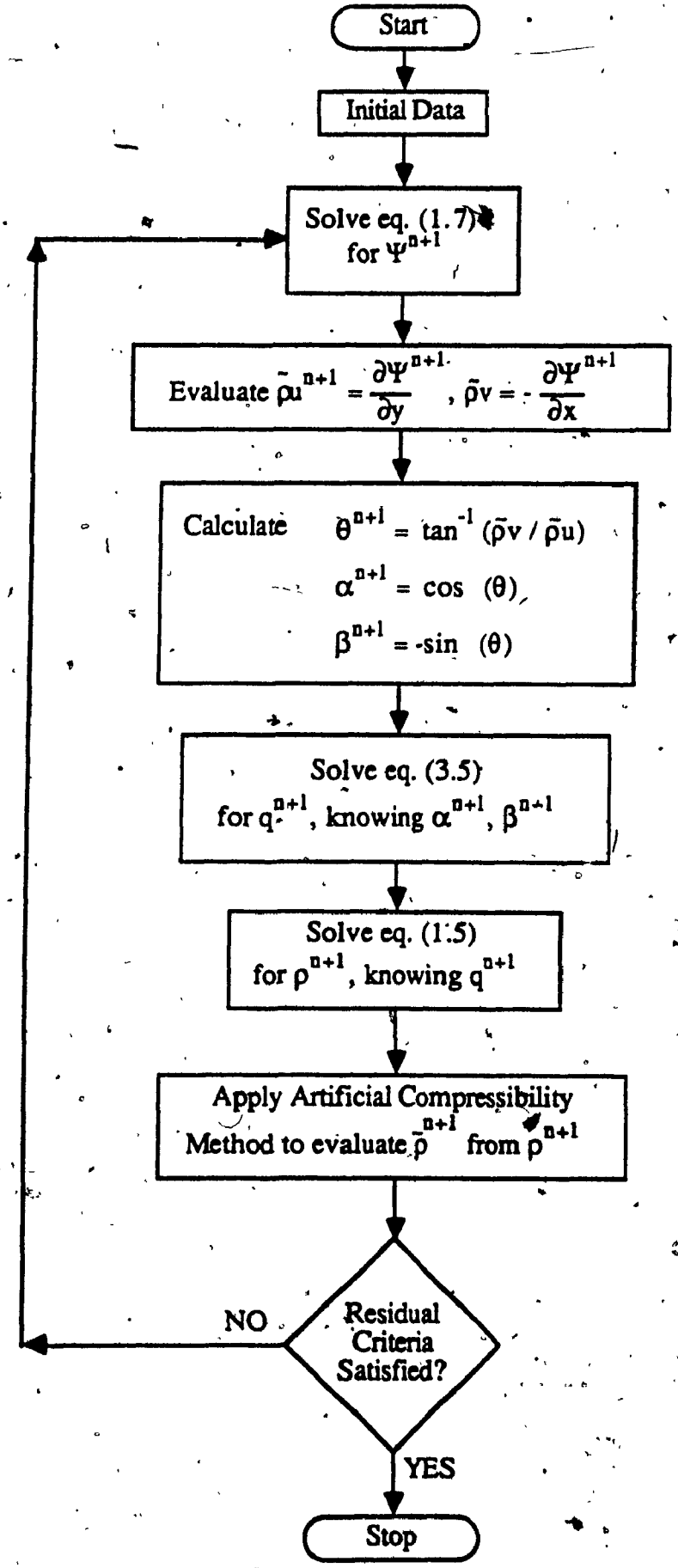

Fig. 3.1 Flowchart for Second Order Vorticity Method

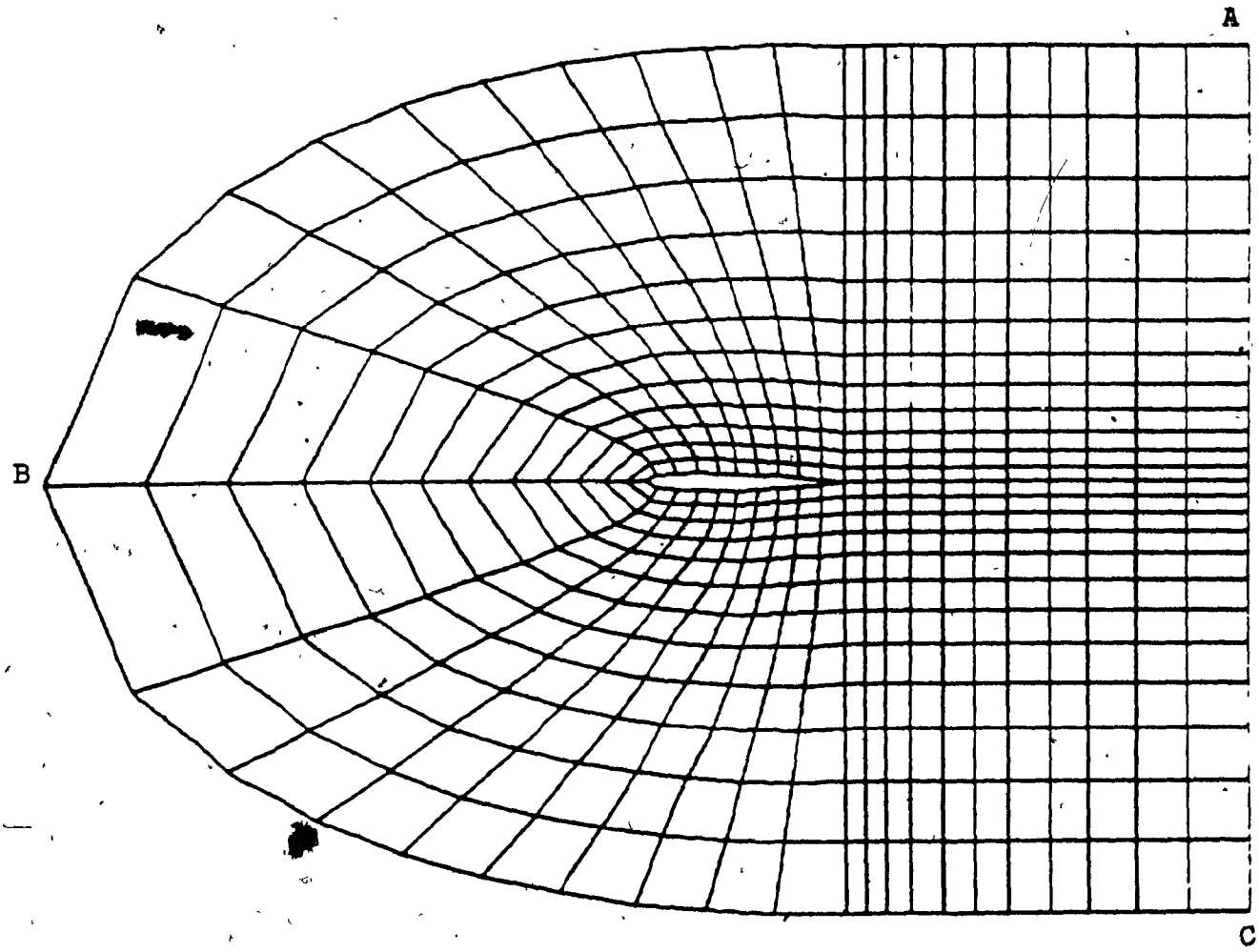

Fig. 3.2 Typical C-Grid Used in Second Order Vorticity Method

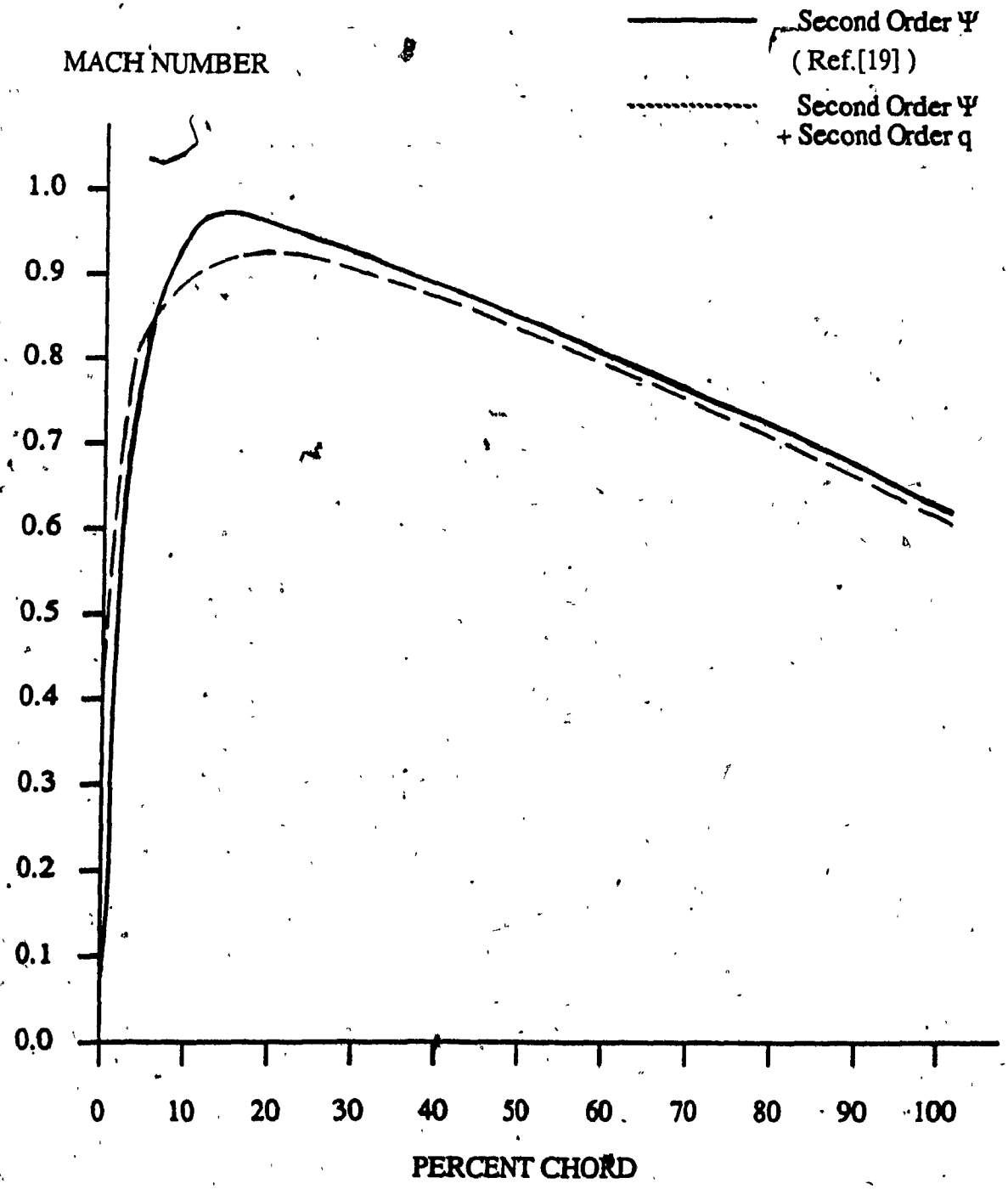

Fig. 3.3 Mach Number vs. Percent Chord for NACA 0012 Airfoil, Second Order Vorticity Method, $M_\infty = 0.72$

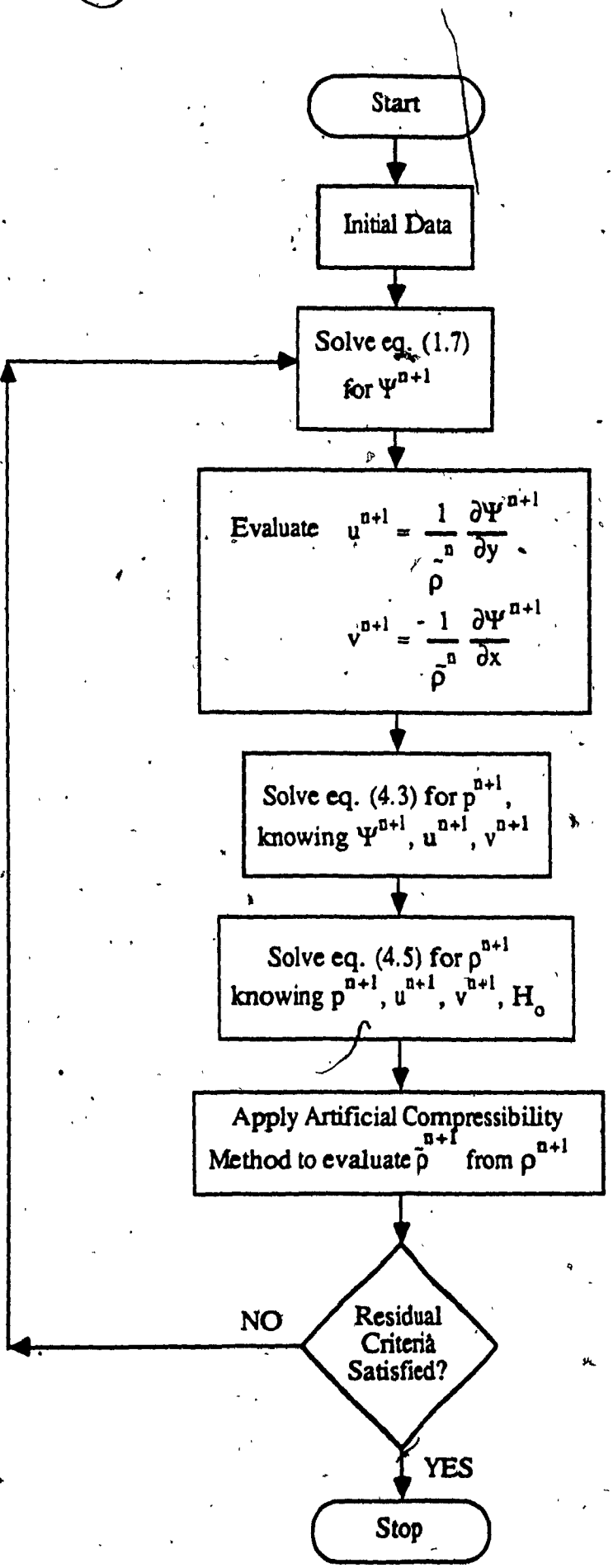

Fig. 4.1 Flowchart for Stream Function and Pressure Method

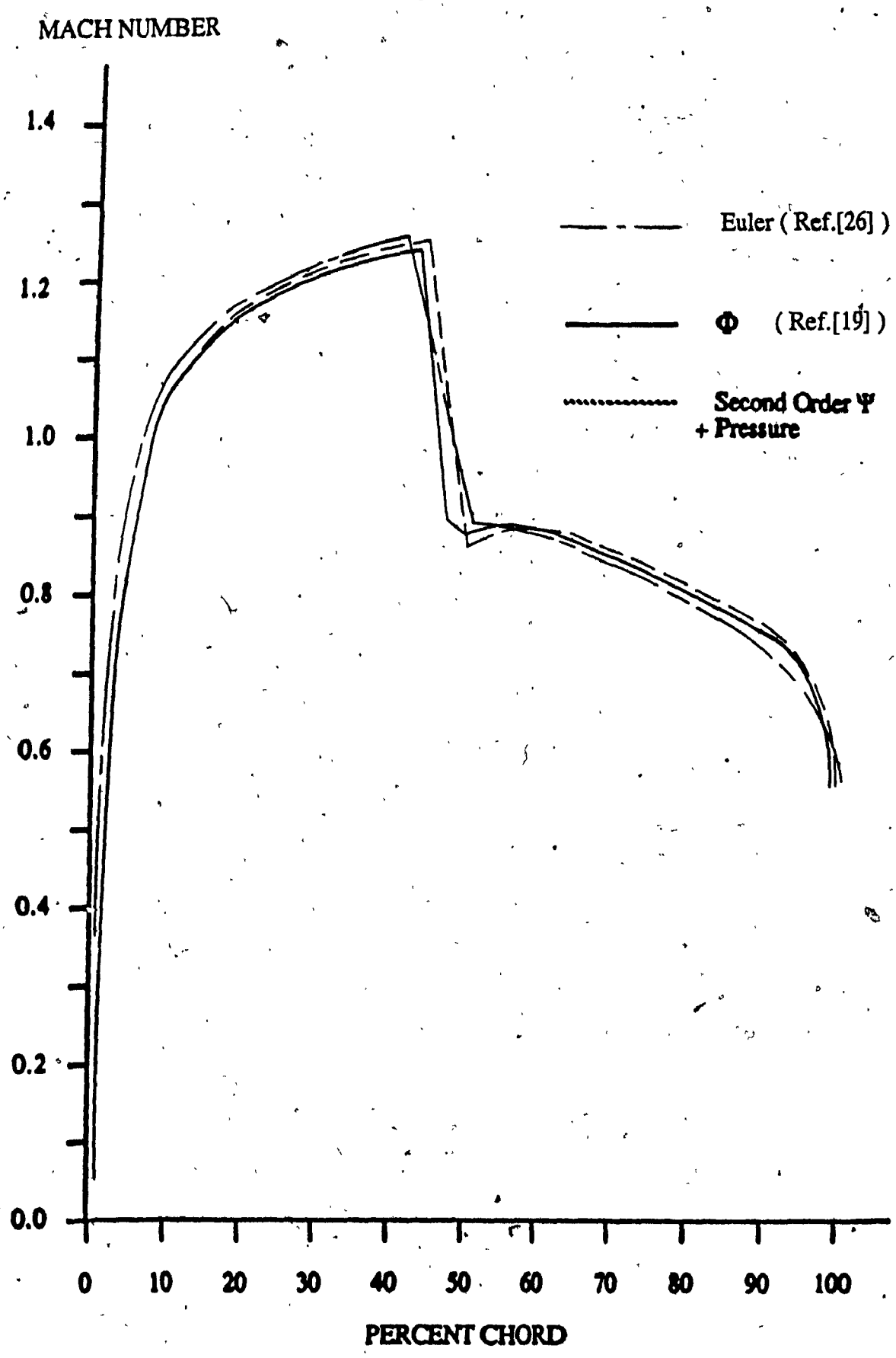

Fig. 4.2 Mach Number vs. Percent Chord for NACA 0012 Airfoil,

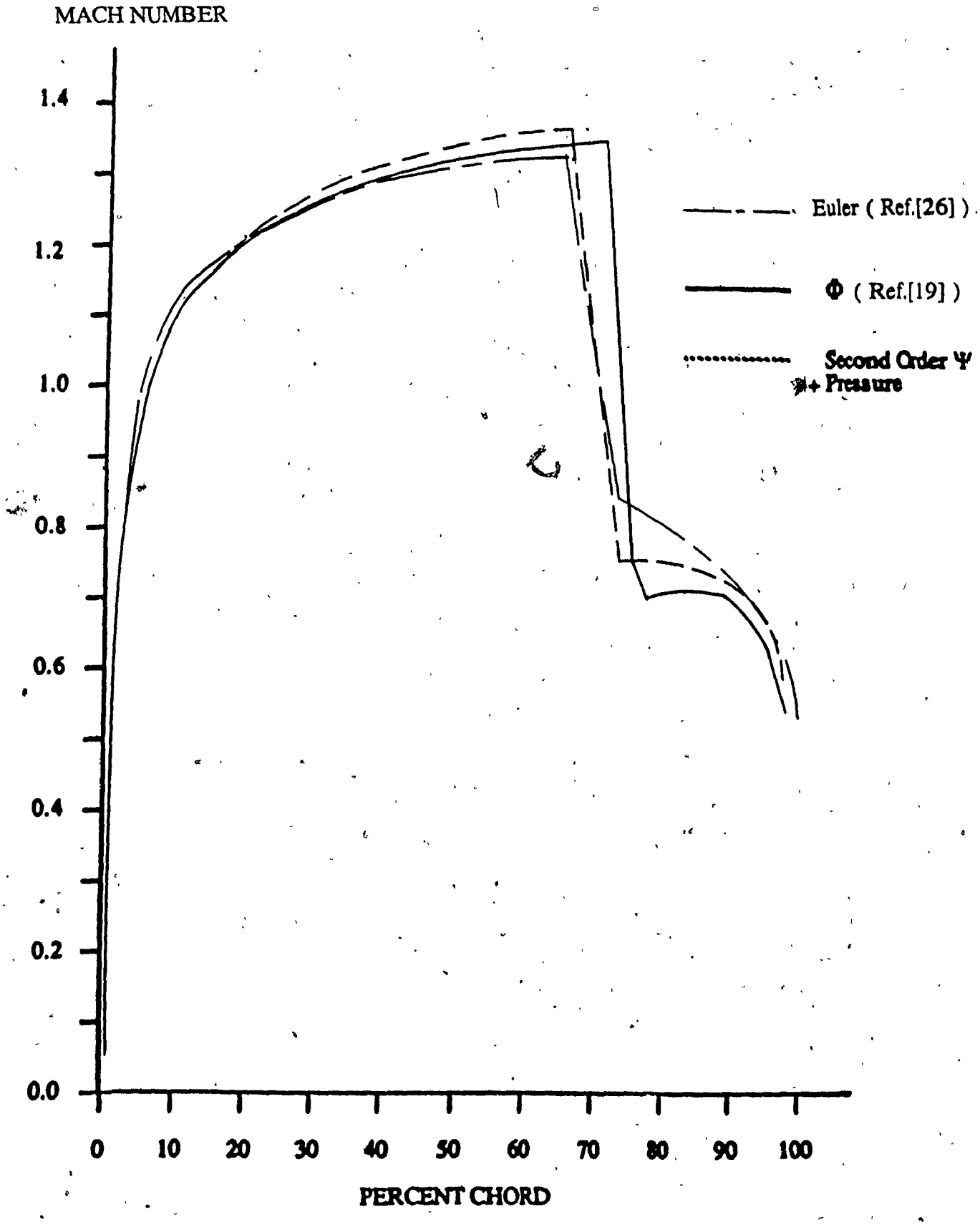

Fig. 4.3 Mach Number vs. Percent Chord for NACA 0012 Airfoil, Stream Function and Pressure Method, $M_\infty = 0.85$

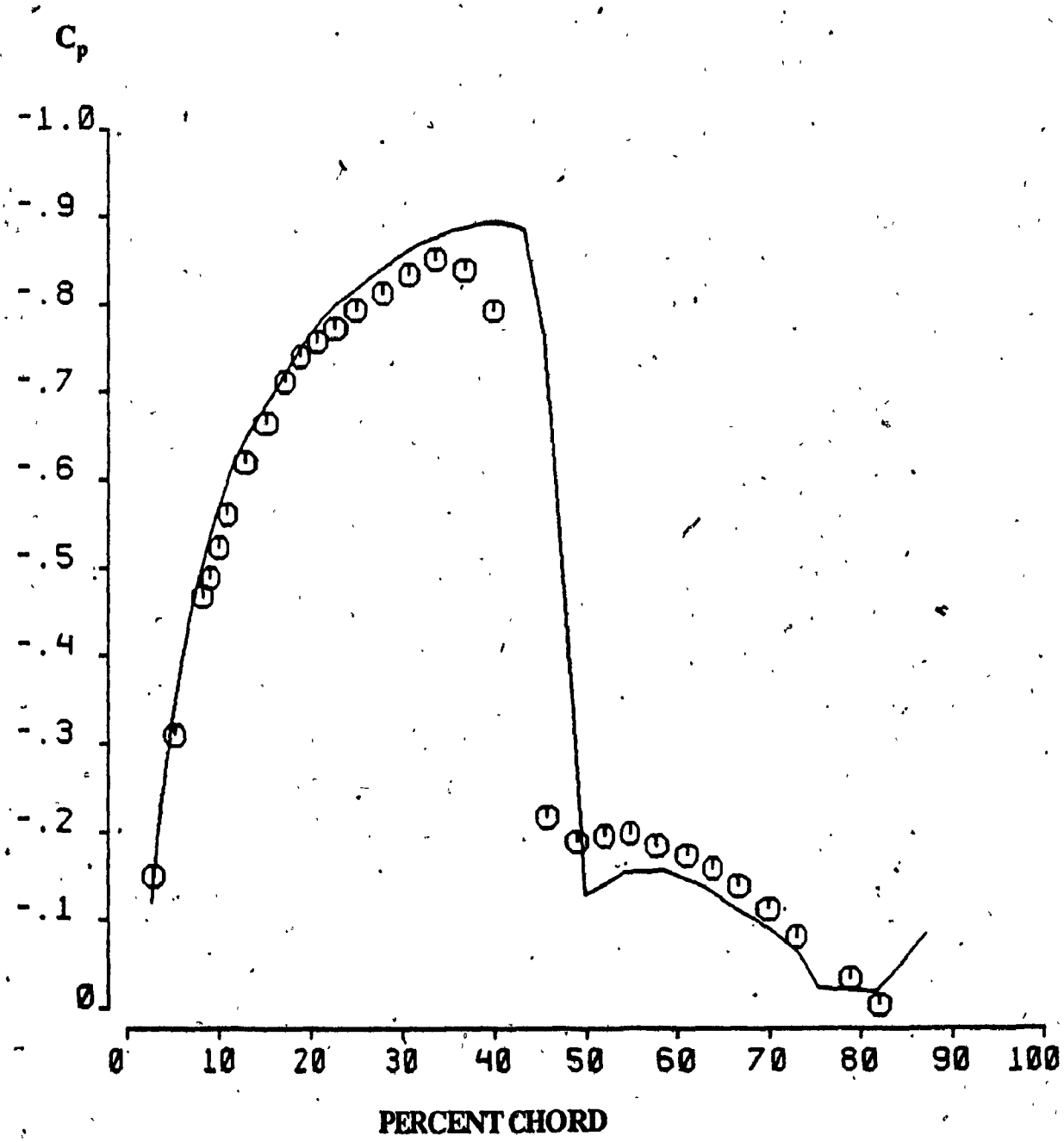

Fig. 4.4 Pressure Coefficient Distribution for NACA 0012 Airfoil, Stream Function and Pressure Method, $M_\infty = 0.80$